CANCER

Neutralization of NET-associated human ARG1 enhances cancer immunotherapy

Stefania Canè[1]†, Roza Maria Barouni[1]†, Marina Fabbi[2], John Cuozzo[3], Giulio Fracasso[1], Annalisa Adamo[1], Stefano Ugel[1], Rosalinda Trovato[1]‡, Francesco De Sanctis[1], Mauro Giacca[4], Rita Lawlor[5], Aldo Scarpa[5,6], Borislav Rusev[5,6], Gabriella Lionetto[7], Salvatore Paiella[7], Roberto Salvia[7], Claudio Bassi[7], Susanna Mandruzzato[8,9], Silvano Ferrini[2], Vincenzo Bronte[9]*

Myeloid cells can restrain antitumor immunity by metabolic pathways, such as the degradation of L-arginine, whose concentrations are regulated by the arginase 1 (ARG1) enzyme. Results from preclinical studies indicate the important role of arginine metabolism in pancreatic ductal adenocarcinoma (PDAC) progression, suggesting a potential for clinical application; however, divergent evolution in ARG1 expression and function in rodents and humans has restricted clinical translation. To overcome this dichotomy, here, we show that neutrophil extracellular traps (NETs), released by spontaneously activated neutrophils isolated from patients with PDAC, create a microdomain where cathepsin S (CTSS) cleaves human (h)ARG1 into different molecular forms endowed with enhanced enzymatic activity at physiological pH. NET-associated hARG1 suppresses T lymphocytes whose proliferation is restored by either adding a hARG1-specific monoclonal antibody (mAb) or preventing CTSS-mediated cleavage, whereas small-molecule inhibitors are not effective. We show that ARG1 blockade, combined with immune checkpoint inhibitors, can restore $CD8^+$ T cell function in ex vivo PDAC tumors. Furthermore, anti-hARG1 mAbs increase the frequency of adoptively transferred tumor-specific $CD8^+$ T cells in tumor and enhance the effectiveness of immune checkpoint therapy in humanized mice. Thus, this study shows that extracellular ARG1, released by activated myeloid cells, localizes in NETs, where it interacts with CTSS that in turn cleaves ARG1, producing major molecular forms endowed with different enzymatic activity at physiological pH. Once exocytosed, ARG1 activity can be targeted by mAbs, which bear potential for clinical application for the treatment of PDAC and require further exploration.

INTRODUCTION

Pancreatic ductal adenocarcinoma (PDAC) is a leading cause of cancer-related deaths in the United States, with a current 5-year survival rate of only 10% (*1*). Most patients present with late-stage metastatic disease, and even patients diagnosed at earlier stages, who are eligible for potentially curative tumor resection, have disease recurrence rates exceeding 80% (*2*). Standard-of-care cytotoxic therapies only modestly extend life expectancy (*3*, *4*); thus, different therapeutic combinations are urgently needed.

Immunotherapies targeting immune checkpoint molecules have transformed clinical outcomes for patients with many types of solid tumors; however, these have yet to affect outcomes for PDAC (*5*), except in a minority of patients harboring microsatellite instability–high tumors (*6*). Poor immunogenicity of PDAC, a highly immunosuppressive tumor immune microenvironment (TME), and dense stroma represent hurdles to immunotherapeutic efficacy (*7*). A more nuanced understanding of the human PDAC immune contexture and immune heterogeneity is needed to inform rational drug combinations and to more effectively stratify patients for immunotherapies to which they are most likely to respond.

Recent development of innovative multiplexed imaging strategies (*8*, *9*) now enables in situ phenotyping and spatial characterization of multiple cell populations simultaneously, thereby facilitating advances in our understanding of the cellular composition of tumors. For example, recent studies in PDAC have revealed extensive T and myeloid cell heterogeneity where spatial localization holds prognostic value (*10*–*12*), supporting the need for further investigations integrating spatial and functional analysis of both adaptive and innate components of the PDAC TME. Recently, quantitative mass spectrometry (MS)–based proteomics detailed extracellular matrix (ECM) changes in both abundance and complexity of proteins in the course of PDAC progression (*13*). Among these changes, several cathepsins, such as B, D, and S (*14*), were found to be up-regulated during the transition from in situ carcinoma to overt PDAC. Moreover, PDAC often contains a tumor microenvironment enriched in suppressive myeloid cells, including neutrophils and fibroblasts, which contribute to maintain an immunosuppressive environment (*15*, *16*).

Tumors drive a tolerant microenvironment characterized by a plethora of immunosuppressive mechanisms (*17*). Among them, the depletion of L-arginine (L-Arg), whose concentration is mainly controlled by arginase 1 (ARG1) and inducible nitric oxide synthase (NOS_2) enzymes (*18*), can have a multifaceted impact on antitumor T lymphocytes (*19*). We recently found that the transfer of tumor-specific cytotoxic T lymphocytes to tumor-

[1]Department of Medicine, Section of Immunology, University of Verona, Verona 37129, Italy. [2]Ospedale Policlinico San Martino, IRCCS, Genova16132, Italy. [3]ZebiAI Therapeutics Inc., Waltham, MA 02467, USA. [4]King's College, London WC2R 2LS, UK. [5]ARC-Net Centre for Applied Research on Cancer, University and Hospital Trust of Verona, Verona 37134, Italy. [6]Department of Diagnostic and Public Health, University of Verona, Verona 37134, Italy. [7]General and Pancreatic Surgery, Pancreas Institute, University of Verona, Verona 37134, Italy. [8]Dipartimento di Scienze Chirurgiche Oncologiche e Gastroenterologiche, University of Padova, Padova 35122, Italy. [9]Istituto Oncologico Veneto IRCCS, Padova 35128, Italy.
†These authors contributed equally to this work.
‡Present address: Merck Group, Ivrea, Italy.
*Corresponding author. Email: vincenzo.bronte@iov.veneto.it

bearing mice, carrying a conditional myeloid ARG1 deficiency, resulted in stronger antitumor immunity and increased overall survival. In contrast, the production of nitric oxide (NO) by NOS_2 enzyme was necessary for the therapeutic benefit of the adoptive cell transfer (ACT) (*18*). Therefore, preferential L-Arg metabolism by ARG1 and not by NOS_2 exerts a negative influence on in vivo antitumor immunity. L-Arg directly modulates T cell metabolism by enhancing cell survival and antitumor activity (*19*); henceforth, the balance to control this amino acid might be crucial for effective immunotherapy.

After the discovery of arginase in mammals, the knowledge about this enzyme and its role in disease pathophysiology has been steadily growing (*20*). Since the 1990s, the structure of arginase and its catalytic mechanism were explored by x-ray crystallography (*21*), paving the way for an intense research program to discover potent and selective arginase inhibitors (*22*–*24*). A growing body of evidence suggests that different cells and tissues, such as the liver and immune system, control ARG1 amount by integrating compartmentalization, gene expression, and protein-protein interactions, therefore strengthening the need to acquire a deeper knowledge about the biology of this enzyme.

Additional complexity is given by the profound evolutionary divergences in the enzyme biology between rodents and humans. Whereas in mice ARG1 is a cytosolic enzyme mainly activated in monocytes and macrophages, in humans, ARG1 isoform 2 is stored in polymorphonuclear (PMN) tertiary granules, whose exocytosis is induced by different stimuli (*25*). By immunoblot analysis, ARG1 appears as a doublet, according to the presence of a leader sequence that drives the protein inside the neutrophil′s tertiary granules. This sequence can be either lost or maintained, depending on the protein cellular compartmentalization (*26*), resulting in two molecular weight bands of 36 and 38 kDa, typical of the full-length ARG1. In addition, an alternative isoform (UniProt isoform 3, 303 amino acids) was identified that might also be expressed in neutrophils, although there are no clear indications so far. Furthermore, secreted ARG1 is active as a full-length protein at alkaline pH, whereas it is inactive at physiological pH unless cleaved by PMN-derived proteases (*27*). These differences among species might have a profound impact on the clinical translation of results achieved in conventional mouse models.

Activated PMNs are known to release neutrophil extracellular traps (NETs), DNA web-like structures enriched in several granule proteins and required to confine microorganisms during infection (*28*). NETosis is a programmed cell death distinct from apoptosis and necrosis. Neutrophils undergoing NETosis are negative for annexin V, a hallmark of apoptosis, but they can switch from NETosis to apoptosis under specific cell signaling conditions (*29*–*31*). Recent studies have shown that NET release is associated with increased metastasis formation (*32*, *33*); however, NETs' contribution to immunosuppression and metastatic spread in human tumors remains largely unknown. Whereas histones, such as H3 and citrullinated H3, together with myeloperoxidase (MPO) and neutrophil elastase, are well-characterized markers of NETosis, nothing is known about the presence of ARG1 and its interaction with other NET components, such as proteases.

Cathepsins are a large family of proteases whose activities range from antimicrobial effects to antigen presentation. Particularly, cathepsin S (CTSS) is a cysteine protease involved in the antigen presentation by major histocompatibility complex II molecules (*34*), degradation of the ECM (*35*), inflammatory diseases (*36*), and tumor progression (*37*). Of note, CTSS is synthesized as a preprotein of 37 kDa whose activation leads to the generation of a mature form (25 kDa), which is active over a broad range of pH, including physiological pH, differently from other members of the family, such as cathepsin G (CTSG). Cysteine cathepsins are overexpressed in cancer (*38*, *39*) and secreted into the tumor extracellular milieu, both by tumor and stromal cells, resulting in a potent degradative activity over a broad range of ECM components, including collagen and laminins (*40*, *41*). In a mouse model of sporadic pancreatic carcinogenesis, the genetic ablation of either cathepsin B or CTSS attenuated tumor invasion and angiogenesis, whereas either cathepsin L or cathepsin B deficiency inhibited tumor proliferation (*42*), highlighting cathepsins′ potential as therapeutic targets for cancer treatment (*43*, *44*). However, given the role that these proteases play in normal immune homeostasis, such as antigen processing and presentation, an approach that targets specific cathepsins with limited normal tissue distribution may be therapeutically more attractive (*45*).

Pharmacological targeting of ARG1 has been focused on amino acid–derived small molecules that enter and bind residues within the active site (*46*). One avenue for targeting of ARG1 is the use of neutralizing antibodies (Abs). Monoclonal antibodies (mAbs) excel in their ability to bind antigens with high specificity, but they lack the ability to access the narrow cleft and active pocket of enzymes, mainly because of their steric hindrance. Recently, Abs toward full-length hARG1 were characterized (*47*), highlighting that alternative mechanisms for ARG1 inhibition are suitable, effective, and need to be further investigated. In this study, we examined the molecular biology of ARG1 in human neutrophils, showing that NETs are enriched in CTSS-cleaved ARG1 forms that specifically contribute to immunosuppression, which is efficiently neutralized by specific mAbs with potential to be combined with immunotherapy treatments for the treatment of PDAC.

RESULTS

In patients with PDAC, constitutively active neutrophils release NETs enriched with different molecular forms of ARG1

NETs are important for directly promoting tumor cell growth, awakening, and metastasis (*33*); however, little is known about the NET contribution to immunosuppression and antitumor immune response. We isolated low-density (LDNs) and normal-density (NDNs) $CD66b^+$ neutrophils from the peripheral blood (PB) of patients with PDAC. Only NDNs can be collected from healthy donors (HDs), because they lack the LDN population (Table 1). After cell purity assessment, cells were rested for 12 hours without any stimulation, and NET formation was evaluated as DNA-MPO complexes. As shown in Fig. 1A, both neutrophil subsets from patients with PDAC released NETs, in contrast to HD neutrophils. In addition, LDNs formed fewer NETs than NDNs, despite both having similar proportions of cell death by apoptosis (fig. S1A). NET-associated ARG1 was not substantially different between the neutrophil subsets (Fig. 1B) and represented the most abundant fraction of total released ARG1 (fig. S1B). When ARG1 activity was evaluated, NETs from both subsets contained the most active enzyme at physiological pH but the lowest at alkaline pH in comparison with ARG1 in either supernatant (SN) or cell

Table 1. Clinical characteristics of the PDAC patient cohort and healthy donor control group evaluated in this study. Patients with PDAC and HDs cohorts: Reported are the gender (%), age, tumor stage, and site of the tumor mass within the pancreas (head, body, and tail). An association of the primary tumor location with survival has been hypothesized.

	Patient cohort (n = 52)	HD cohort (n = 52)
Gender		
Female	45.3%	39.6%
Male	32.7%	60.4%
Age	44–86 (average 65)	44–86 (average 63.5)
Stage		
IV	36.9	
III	48.6	
IIA and IIB	14.5	
Tumor site		
Head	75.8	
Body	18.9	
Tail	5.5	

pellet (Fig. 1C and fig. S1C-D). We reasoned that ARG1 might be present in different molecular forms in NETs. Therefore, we performed immunoblots of ARG1 in NETs obtained from LDNs and NDNs. As shown in Fig. 1D, besides the expected molecular forms at 38 and 36 kDa, we observed a band of 31 kDa, suggesting potential cleavage of ARG1. Because ARG1 has been associated with the suppression of activated T lymphocytes, we next evaluated whether this molecular pattern affected ARG1-dependent immunosuppressive function. We observed that proliferation of activated T cells was reduced in NETs from both LDNs and NDNs. Treatment with ARG1-blocking mAb restored the proliferation of T cells, whereas commercially available ARG1 small-molecule inhibitors, such as *N*-hydroxy-nor-L-arginine (nor-NOHA) and *S*-2-boronoethyl-L-cysteine (BEC), were ineffective (Fig. 1, E and F). Moreover, the blocking mAb was ineffective in restoring the proliferation of T lymphocytes when cultured with LDNs and NDNs as whole cells, whereas small-molecule inhibitors rescued cell-mediated suppression (fig. S1, E and F). Collectively, these results demonstrate that neutrophils from patients with cancer constitutively release NETs carrying different molecular forms of ARG1 endowed with immunosuppressive functions, which are neutralized by αARG1, but not by small-molecule ARG1 inhibitors.

The presence of activated neutrophils releasing different molecular forms of ARG1 prompted us to evaluate the enzyme concentration and activity in patients′ sera. As shown in Fig. 1G, we found that patients with PDAC had higher amounts of serum NETs and serum ARG1 than HDs (Fig. 1H). ARG1 activity at pH 7.3 was higher in patients with PDAC as compared with HDs, whereas the opposite was true for pH 9.5, indicating a shift in ARG1 function associated with tumor presence (Fig. 1I). Moreover, sera from patients with PDAC suppressed the proliferation of activated T cells, and mAb 1.10 restrained this activity (Fig. 1J). We attempted to identify the systemic factors triggering neutrophil activation by focusing on interleukin-8 (IL-8) and tumor necrosis factor-α (TNF-α), known neutrophil activators (*48*); furthermore, increased concentrations of IL-8 in the sera of patients with cancer have been associated with impaired benefits of checkpoint inhibitors (*49*). Both IL-8 and TNF-α were higher in the sera of patients with PDAC than in those of HDs (Fig. 1K).

We next asked whether ARG1 cleavage and localization observed in patients with PDAC also occurred in stimulated PMNs from HDs. Depending on the type of degranulating stimuli, PMNs undergo NETosis (*50*), and ARG1 is exocytosed (*25*). However, whether exocytosed ARG1 localizes in NETs is not yet defined. We performed confocal microscopy on PMNs isolated from PB of HDs, either stimulated with ionomycin or left untreated (media) (fig. S2, A and B). A time-dependent increment in NETs was observed, with the early stage of NETosis characterized predominantly by granule-restricted expression of ARG1; at a later stage (2 hours), cells increased their size, and ARG1 was coexpressed together with MPO along the network of NET chromatin strands (fig. S2, A and B). Similar results were also obtained when PMNs were stimulated with phorbol-12-myristrate-13-acetate (PMA) and molecules relevant for neutrophil activation, degranulation, and chemotaxis (fig. S2, C and D), including IL-8 and TNF-α, which are increased in sera of patients with PDAC (Fig. 1K), as well as in different cancers (*49*, *51*, *52*).

ARG1 is stored in PMN tertiary granules as an inactive molecule (*26*), whereas the enzyme released upon PMN exocytosis efficiently catabolizes L-Arg (*53*). Thus, we tested whether ARG1 functional activation, observed in patients with PDAC, might be related to ARG1 forms present in NETs. We isolated and characterized NETs after PMN activation and observed a time-dependent increase in ARG1 low–molecular weight bands (major forms at 31 and 25 kDa; fig. S3A). These bands were only slightly visible in NETs from control PMNs (media, 30 min and 2 hours) (fig. S3A) and completely absent in cell pellet lysates from both activated and control PMNs (fig. S3B, left), as well as freshly isolated PMNs and peripheral blood mononuclear cells (PBMCs; fig. S3B, right). These findings suggest that there is ARG1 protein cleavage in NETs. We then quantified NETs (fig. S3C) and assessed the enzymatic activity in cell pellet lysates and NETs of either stimulated or resting PMNs, at both ARG1 optimal (pH 9.5) and physiological (pH 7.3) pH. At pH 9.5, we observed a time-dependent increase in the enzymatic activity, with a 2-hour stimulation reaching an overall similar activity in both NETs and cell lysates (fig. S3D). Conversely, ARG1 enzyme activity was detectable almost exclusively in NETs when assessed at pH 7.3 (fig. S3E). These results argue that the cleaved forms of ARG1 are associated with an enzyme gain of function at physiological pH. We next evaluated whether NET-derived ARG1 is endowed with immune regulatory activity. NETs from stimulated PMNs, containing ARG1 (fig. S3F), were collected and the physiological L-Arg concentration (150 μM) was restored before adding this preparation to activated T cells. ARG1 from NETs suppressed T lymphocyte activation by anti-CD3/anti-CD28, as shown by the down-regulation of CD3ε (fig. S3G). We then evaluated the effect on T cell proliferation in the presence of the blocking mAbs directed against hARG1 or isotype [immunoglobulin G1 (IgG1)] controls. Comparable to patients with PDAC, the αARG1 restored T cell proliferation (fig. S3H), whereas small-molecule BEC and nor-NOHA were ineffective or slightly effective, respectively (fig. S3I). Moreover, nor-NOHA and BEC are not effective against NET-associated ARG1, yet these small-molecule inhibitors rescued the inhibition of

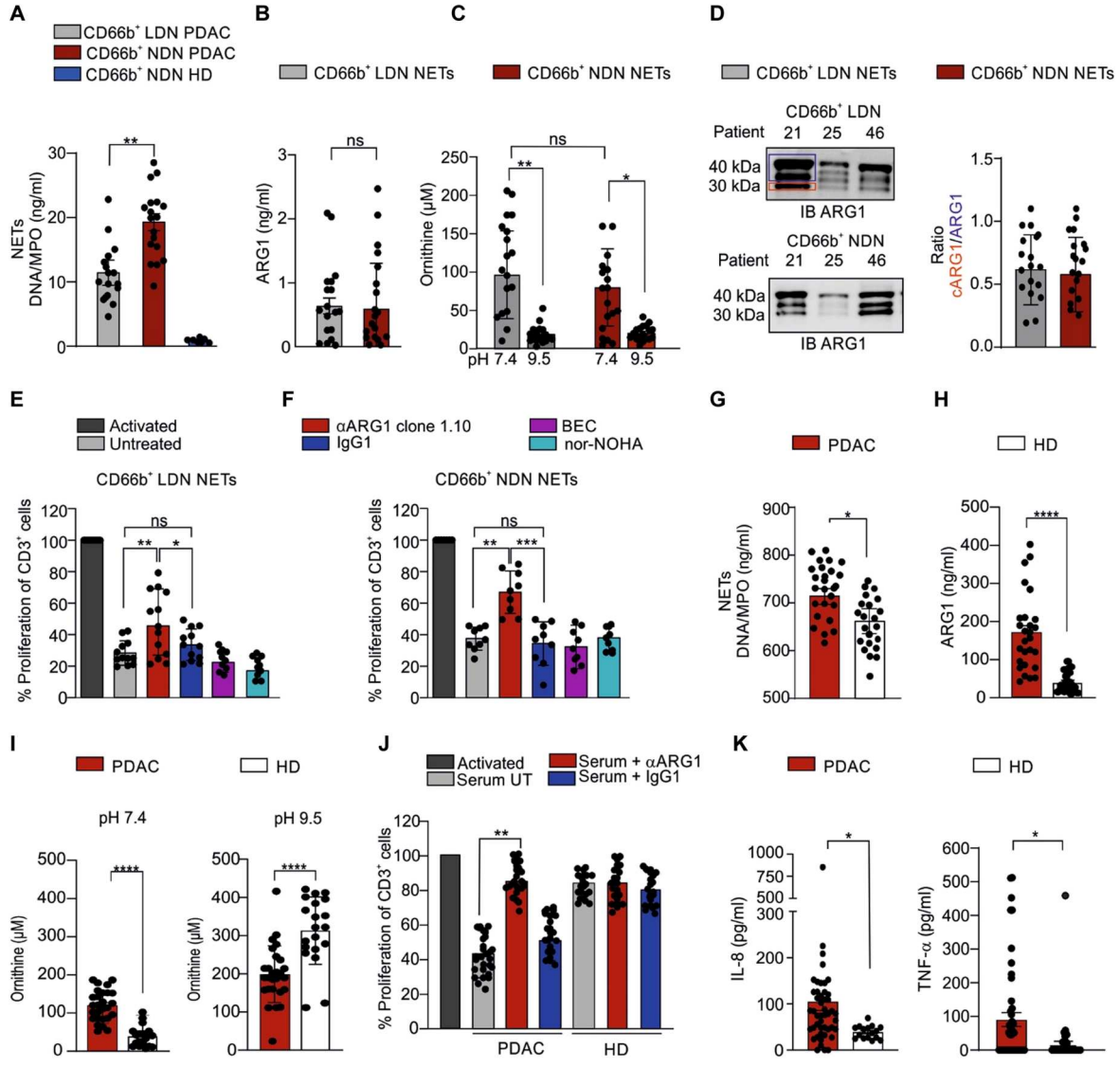

Fig. 1. Blockade of NET-associated ARG1 by mAbs reduces the immune suppressive activity of PMNs and sera from patients with PDAC. (**A**) Quantification of DNA-myeloperoxidase (MPO) complex concentration (ng/ml) by ELISA in neutrophil extracellular trap (NET)–enriched supernatants (SNs) of CD66b$^+$ low-density neutrophils (LDNs) and CD66b$^+$ normal-density neutrophils (NDNs) from patients with PDAC ($n = 18$) and CD66$^+$ NDNs from HDs ($n = 7$). The data are presented as mean ± SEM. Unpaired, two-tailed, Student's t test. $^{**}P = 0.0023$. (**B**) Quantification of ARG1 concentration (ng/ml) by ELISA in NET-enriched SNs of CD66b$^+$ LDN and CD66b$^+$ NDN cells from patients with PDAC ($n = 18$). The data are presented as means ± SEM. Paired, two-tailed, Student's t test. ns, not significant. (**C**) Determination of ARG1 activity in NETs of CD66b$^+$ LDN ($n = 18$) and CD66b$^+$ NDN cells ($n = 18$) from patients with PDAC. Ornithine concentration is evaluated by colorimetric assay at pH 7.3 and at pH 9.5. The data are presented as means ± SEM. One-way ANOVA, multiple comparisons, and Tukey's post hoc correction. $^*P < 0.032$ and $^{**}P = 0.0017$. (**D**) Representative immunoblots showing ARG1 molecular pattern in NETs of CD66b$^+$ LDN (top) and CD66b$^+$ NDN cells (bottom). Histogram shows quantification of ARG1-FL and ARG1-31, represented as a ratio ARG1-31/ARG1-FL, in NETs of CD66b$^+$ LDN ($n = 18$) and CD66b$^+$ NDN cells ($n = 18$). ARG1-31 band is shown inside the red box, and ARG1-FL is included in the blue box. The data are presented as means ± SEM. (**E** and **F**) Proliferation assay showing the percentage of anti-CD3 and anti-CD28–activated T cells, cultured with cell-derived suppressive NET-containing conditioned medium (E, CD66b$^+$ LDN, $n = 13$; F, CD66b$^+$ NDN, $n = 9$). T cells were cultured with either αARG1 (150 μg/ml), IgG1 isotype control (150 μg/ml), BEC (10.5 ng/ml), or nor-NOHA (30 ng/ml). Activated T cells were set as 100% proliferation and used as control. Suppressive activity is represented as the percentage of proliferation of CD3$^+$ CellTrace$^+$ cells. The data are presented as means ± SEM. One-way ANOVA, multiple comparisons, and Tukey's post hoc correction. $^*P < 0.05$; $^{**}P < 0.01$; $^{***}P = 0.001$. (**G**) Quantification of DNA-MPO complex concentration (ng/ml) by ELISA in sera of patients with PDAC ($n = 26$) and of HDs ($n = 21$). The data are presented as means ± SD. Unpaired, two-tailed, Student's t test. $^*P < 0.05$. (**H**) Quantification of ARG1 concentration (ng/ml) by ELISA in sera of patients with PDAC ($n = 26$) and of HDs ($n = 21$). The data are presented as measn ± SEM. Unpaired, two-tailed, Student's t test. $^{****}P < 0.0001$. (**I**) Determination of serum-derived ARG1 activity by colorimetric assay in sera of patients with PDAC ($n = 26$) and of HDs ($n = 21$). The concentration of ornithine obtained at pH 7.3 (left) and pH 9.5 (right) is shown. The data are presented as means ± SEM. Unpaired, two-tailed, Student's t test. $^{****}P < 0.0001$. (**J**) Proliferation assay showing the percentage of anti-CD3– and anti-CD28–activated T cells, cultured with sera from patients with PDAC ($n = 52$) and of HDs ($n = 14$). Sera from patients with PDAC and HDs were either left untreated or incubated with neutralizing αARG1 (150 μg/ml) or IgG1 isotype control. Activated T cells were set as 100% proliferation and used as a control. Suppressive activity is represented as the percentage of proliferation of CD3$^+$ CellTrace$^+$ cells. The data are presented as means ± SEM. Unpaired, two-tailed, Student's t test. $^{**}P = 0.0045$. (**K**) Quantification by ELISA of IL-8 (left) and TNFα (right) concentration in sera of patients with PDAC ($n = 52$) and HDs ($n = 14$). The data are presented as means ± SEM. Unpaired, two-tailed, Student's t test. $^*P < 0.05$.

full-length rhARG1 on T cell activation (fig. S3J), suggesting that the uncleaved rhARG1 might be biochemically and functionally distinct from the cleaved, NET-associated forms.

CTSS interacts with and cleaves ARG1 in NETs of activated PMNs

To identify the protease responsible for the cleavage in the NETs, we defined ARG1-interacting proteins by coimmunoprecipitation (co-IP) of ARG1 with the mAb 1.10. After we loaded the IP preparation onto an SDS–polyacrylamide gel electrophoresis, the region of gel containing the proteins was excised and subjected to liquid chromatography–tandem MS (LC-MS/MS) upon validation that ARG1 was successfully pulled down (Fig. 2A). Among several identified, interacting proteins (Table 2), we focused on CTSS as a suitable protease candidate. CTSS is cysteine protease enriched in the ficolin/secretory granules (*26*) and is active and stable at physiological pH. We validated the proteomic data by ARG1 co-IP (Fig. 2B and fig. S4A) and immunofluorescence (IF) staining (Fig. 2, C and D, and fig. S4B), which confirmed the colocalization of ARG1 and CTSS on both nicotinamide adenine dinucleotide phosphate–dependent (PMA-induced; fig. S4, C and D) and nicotinamide adenine dinucleotide phosphate–independent (ionomycin-induced) NETs (Fig. 2C and fig. S4B). This was further supported by the presence of CTSS in NETs (Fig. 2E). Because CTSS is active at physiological pH, we next determined whether full-length rhARG1 was a substrate for recombinant human cathepsin S (rhCTSS). Isothermal calorimetry (ITC) analysis revealed that the binding of pro-CTSS (Fig. 2F, left), which is proteolytically inactive, to rhARG1 is thermodynamically favorable (Table 3), profiling an interaction of one rhARG1 monomer binding to a single site on pro-CTSS, with a dissociation constant (K_d) in the micromolar range. When mature CTSS was incubated with rhARG1 (Fig. 2F, right, and Table 3), the enthalpy variation (ΔH) became more negative but was compensated by an increase in entropy variation (ΔS), which led to a net result of no change in free energy and binding affinity compared

Table 2. ARG1-interacting proteins identified in NETs of stimulated PMNs by LC-MS/MS. The analysis of the coimmunoprecipitated proteins in NETs revealed a list of the potential proteins interacting with hARG1. In the table, details concerning the obtained peptides (total number and unique peptides), peptide spectrum matches (PSMs), peptide coverage, and a brief description of the protein function are included. GAPDH, glyceraldehyde-3-phosphate dehydrogenase; CTP, cytidine 5′-triphosphate; GTP, guanosine 5′-triphosphate; ATP, adenosine 5′-triphosphate; MAPK, mitogen-activated protein kinase.

Protein ID	Protein description	Unique peptides	Peptides	PSms	Coverage	Major biological processes
P04406	GAPDH	5	5	14	14.33	Glycolysis; antimicrobial defense; microtubule organization; nitrosilace activity
P02788-2	Isoform delta lactotransferrin	8	8	20	13.21	Antimicrobial; defense response
P17213	Bactericidal permeability-increasing protein	3	3	4	6.37	Antimicrobial response
P20160	Azurocidin	2	2	10	8.37	Antimicrobial; cell extravasation; chemotaxis; inflammatory response
P08246	Neutrophil elastase	3	3	11	7.12	Inflammatory response; extracellular matrix remodeling
P15531	Nucleoside diphosphate kinase A	2	2	2	20.39	Synthesis of CTP and GTP, negative regulator of cell proliferation
U3KQE7	Cathepsin S	3	3	8	23.08	Antigen presentation; proteolysis; collagen degradation
P05164-2	Isoform H14 of myeloperoxidase	8	8	20	12.00	Cen redox homeostasis; defense response
P54108	Cysteine-rich secretory protein	2	2	4	6.94	Defense response
P05089	Arginase-1	8	8	29	28.88	Urea cycle; immunoregulation; collagen biosynthesis
C9JEY1	Actin-related protein 2/3 complex subunit 1B	2	2	2	7.78	Arp2/3 complex–mediated actin nucleation
P30740	Leukocyte elastase inhibitor	2	2	4	6.33	Peptidase inhibitor activity; negative regulator of IL-1β secretion
P59665	Neutrophil defensin 1	3	3	19	20.21	Defense response; T cell chemotaxis
Q14917	14-3-3 Protein eta	3	3	3	14.63	G_2-M transition; intracellular signaling; MAPK cascade; membrane organization
Q04075	Fructose-bisphosphonate aldolase A	13	14	42	29.40	Glycolysis; neutrophil degranulation; ATP biosynthetic process
P62258-2	Isoform SV of 14-3-3 protein epsilon	4	4	13	18.88	G_2-M transition; intracellular signaling; MAPK cascade; membrane organization
P09972-2	Fructose-bisphosphonate aldolase C	4	5	11	16.76	Glycolysis; neutrophil degranulation; ATP biosynthetic process
P60709	Actin cytoplasmic 1	13	13	59	26.40	Structural constituent of cytoskeleton

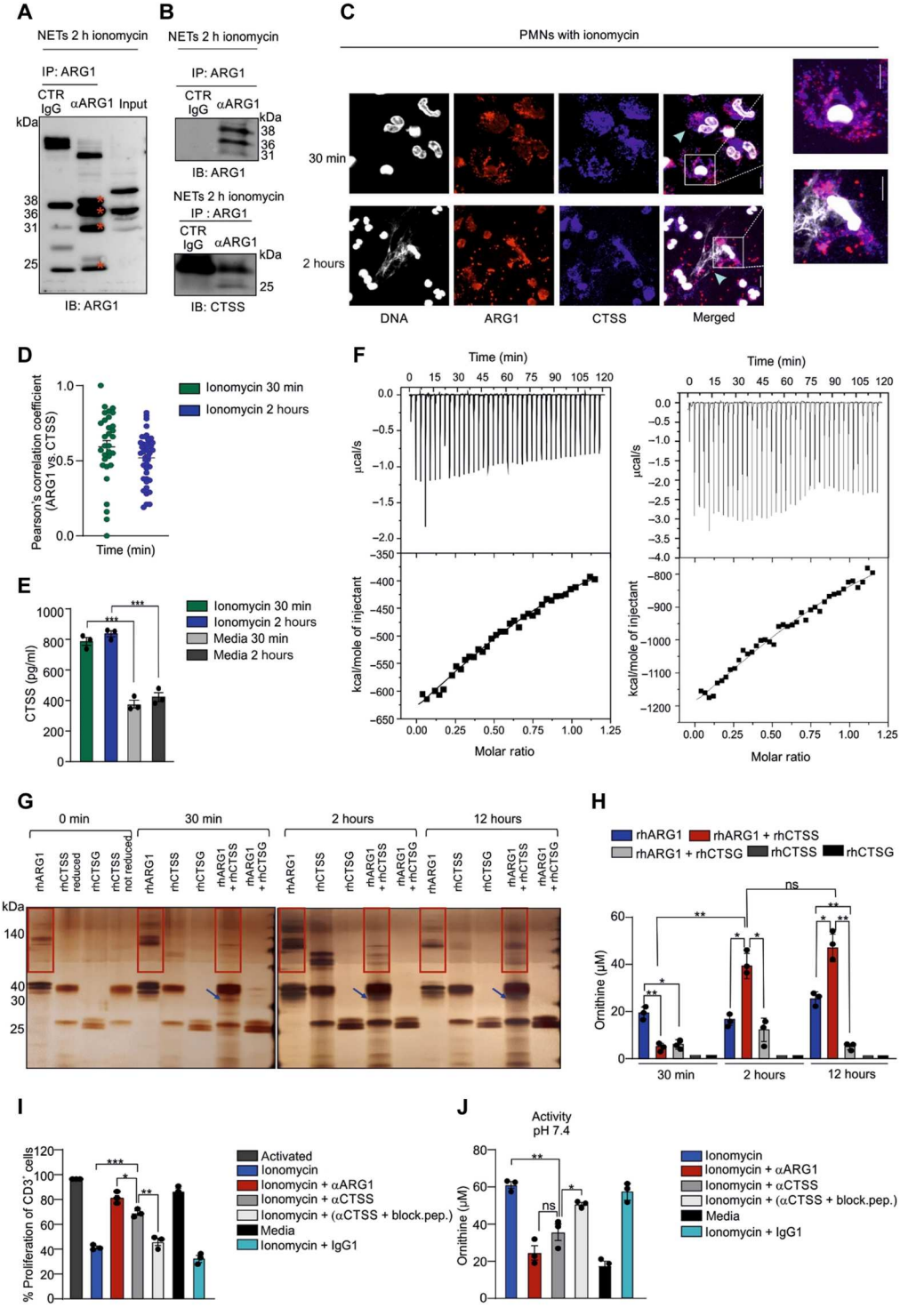

Fig. 2. CTSS interacts with and cleaves ARG1 in NETs of activated PMNs. (**A**) Immunoblot showing ARG1 protein band pattern (38, 36, 31, and 25 kDa; red stars top to bottom) of co-IP ARG1 from NETs of polymorphonuclear cells (PMNs) treated with ionomycin 5 μM for 30 min. Ab αARG1 and IgG1 isotype control are indicated. (**B**) Immunoblot (IB) showing ARG1 (top) and CTSS (bottom) coexpression obtained from co-IP of ARG1 (Ab clone 1.10 or IgG1 control, 2 μg) from NETs of PMNs treated with 5 μM ionomycin for 30 min. (**C**) Representative IF images showing ARG1 (red), CTSS (blue), and DNA (gray) of PMNs treated with 5 μM ionomycin for 30 min and 2 hours. The light blue arrowheads indicate PMNs undergoing NETosis. Shown in the white box is the maximum projection. Scale bars, 10 μm. (**D**) Quantification of ARG1 and CTSS colocalization within the NETs produced at 30 min and 2 hours, ionomycin-treated PMNs. Pearson's correlation coefficient analysis. The data are presented as means ± SEM. (**E**) Quantification of CTSS concentration (ng/ml) by ELISA in NETs produced at 30 min and 2 hours, ionomycin-treated or untreated (media) PMNs ($n = 3$). The data are presented as means ± SEM. Paired, two-tailed, Student's t test. $^{***}P = 0.0003$. (**F**) Isothermal titration calorimetry (ITC) analysis of proCTSS (left) and mature CTSS (right) interactions with rhARG1. The top plots show time (min) versus microcalorie per second, whereas the bottom plots show molar ratio versus kilocalorie per mole of the injectant. (**G**) ARG1 immunoblot showing rhARG1 (200 ng) kinetic digestion (30 min, 2 hours, and 12 hours) in the presence or absence of rhCTSG (800 ng) or rhCTSS (800 ng). Relevant bands are indicated by red boxes and blue arrows. (**H**) Determination of ARG1 activity, represented as ornithine concentration, at pH 7.3 by colorimetric assay in the samples evaluated in G ($n = 3$). The data are presented as means ± SEM. One-way ANOVA, multiple comparisons, and Tukey's post hoc correction. $^{*}P < 0.05$; $^{**}P < 0.01$. (**I**) Proliferation assay showing the percentage of anti-CD3– and anti-CD28–activated T cells cultured with NETs produced at 30 min, in ionomycin-treated PMNs or untreated (media). In some conditions, before the stimulation of PMNs, neutralizing Ab to CTSS (150 μg/ml) was added to the culture. In addition, neutralizing Ab anti-CTSS was preincubated for 30 min with a blocking peptide (1.5 ng/ml), and then the mix was added to PMNs, followed by their activation with 5 μM ionomycin ($n = 3$). Activated T cells were set as 100% proliferation and used as a control. Suppressive activity is represented as the percentage of proliferation of $CD3^+$ $CellTrace^+$ cells. The data are presented as means ± SEM. One-way ANOVA, multiple comparisons, and Tukey's post hoc correction. $^{*}P < 0.05$; $^{**}P < 0.01$; $^{***}P < 0.001$. (**J**) Determination of ARG1 activity at pH 7.3 by colorimetric in the same samples used in (I) ($n = 3$). The data are presented as means ± SEM. One-way ANOVA, multiple comparisons, and Tukey's post hoc correction. $^{*}P < 0.05$; $^{**}P < 0.01$.

Table 3. Thermodynamic constants of rhARG1 and rhCTSS binding. The binding was assessed with rhCTSS as a proprotein and mature form. The thermodynamic parameters were derived from the best fit of ITC profile of proCTSS and active CTSS titrated with ARG1 obtained using a one-site sequential binding model.

Constant	Procathepsin S	Mature cathepsin S
K_d (M)	$2.16 \times 10^6 \pm 1.41. \times 10^{-6}$	$2.10 \times 10^{-6} \pm 1.77 \times 10^{-6}$
ΔH (kcal/mol)	−565 ± 201	−1000 ± 561
$T\Delta S$ (kcal/mol)	557	992

to pro-CTSS. This indicated that full-length rhARG1 and rhCTSS interact independently of rhCTSS proteolytic activity.

We then focused on full-length rhARG1 cleavage by rhCTSS. As shown in Fig. 2G, a time-dependent digestion of rhARG1 by rhCTSS produced cleaved products, such as 31 and 25 kDa (blue arrows), which recapitulated the molecular pattern observed in NETs of activated PMNs (fig. S3A). On the basis of proteomic analysis (Table 4), the 31-kDa band in rhARG1 alone showed a sequence different from the 31-kDa generated after rhARG1 cleavage by rhCTSS. At later time points (2 and 12 hours), the prolonged exposure of rhARG1 to rhCTSS resulted in the appearance of high–molecular weight forms (red boxes), which were characterized by different molecular patterns and composition. The high molecular weight forms appearing upon coincubation of rhARG1 and rhCTSS, at 2 and 12 hours, contained not only ARG1 but also CTSS, as shown by the gel presented in Fig. 2G reblotted for CTSS (fig. S4E). In contrast, the enzymatic activity of another cathepsin family member present in neutrophils, such as recombinant human cathepsin G (rhCTSG) (*39*), resulted in almost complete rhARG1 digestion after 12-hour incubation (Fig. 2G). When we assessed the enzyme activity of rhARG1 in the digestion mix at pH 7.3, we noticed a time-dependent increase only when rhARG1 was incubated with rhCTSS, whereas the activity in the presence of rhCTSG was reduced (Fig. 2H). Having found that ARG1 is a substrate for CTSS, we reasoned that altering CTSS activity, using a neutralizing Ab, might also affect ARG1 activity. The dose-dependent efficacy of the mAb blocking CTSS in vitro was first established, together with the effective concentration of the peptide that interferes with the binding of the mAb to CTSS (fig. S4, F and G). CTSS increased the suppression mediated by full-length rhARG1 on T lymphocytes, and the addition of αARG1, but not small-molecule inhibitors, restored the proliferation of activated T cells (fig. S4H). We then stimulated PMNs in the presence or absence of a neutralizing Ab to CTSS, either alone or preincubated with the blocking peptide. The resulting NETs were added to anti-CD3/anti-CD28–activated, labeled T cells, as before. CTSS blockade restored the proliferation of T cells, although less than direct ARG1 neutralization. Blockade of CTSS activity with the blocking peptide rescued suppression (Fig. 2I). These results were similar to changes in ARG1 enzyme activity (Fig. 2J), supporting the premise that the effects on proliferating T cells were linked to changes in ARG1 function. Therefore, ARG1 and CTSS interact in NETs, and CTSS neutralization was efficient in reducing both enzyme activity and immune suppression mediated by NET-associated ARG1.

ARG1 cleaved form is endowed with different enzymatic properties

We argued that the partial inefficacy of ARG inhibitors on extracellularly released ARG1 could be linked to the presence of alternative molecular forms endowed with different functional activity. We focused on the 31-kDa ARG1 form because it was present in NETs of in vitro–activated neutrophils and PMNs enriched from patients with PDAC. We isolated, sequenced (Fig. 3A), cloned (Fig. 3B), and functionally (Fig. 3C) tested the 31-kDa molecular form (hereafter indicated as ARG1-31). This form shares the C terminus with ARG1 full length, and it is cleaved at amino acid 42 from the N terminus (fig. S5A). ARG1-31 rapidly hydrolyzed L-Arg, with half of the substrate already converted within 11 min (Table 5 and fig. S5B). The mAb 1.10 delayed the enzymatic activity on a molar ratio basis and reached the maximum inhibitory capacity at a 1:30 ratio (Table 5 and fig. S5C). Instead, BEC and nor-NOHA were ineffective at reducing enzymatic activity (fig. S5, D and E). We then asked whether the ARG1-31 inhibited T cell proliferation in vitro. ARG1-31 reached the same extent of suppression achieved with 5 ng/ml of full-length protein at the concentration of just 0.1 ng/ml, which corroborated its enhanced enzymatic function (Fig. 3C, fig. S5B, and Table 5). The mAb 1.10 restored T cell proliferation, whereas BEC and nor-NOHA did not (Fig. 3C), although they blocked the enzymatic activity of full-length ARG1 (fig. S3J).

Because the C terminus of ARG1 is required to support the molecular interactions among monomers to form a stable trimer, we argue that the binding of the Ab to this region might destabilize the assembly of a fully functional quaternary structure. The interference with enzyme activity might thus be independent of the occupancy of the catalytic site. To gain further insight into the three-dimensional structure of ARG1-31, we performed dynamic light scattering analysis. As shown in Fig. 3 (D and E), rhARG1 and

Table 4. Amino acid sequences of ARG1-31 alone and ARG1-31 obtained from coincubation of rhARG1 and rhCTSS. Differences in amino acid sequence between ARG1-31 derived from ARG1 alone and ARG1-31 obtained from in vitro digestion of rhARG1 with rhCTSS (referred to Fig. 2G). The crossed out amino acids are different between the two forms.

Sequence of ARG1-31 kDa not cleaved by CTSS but appearing in rhARG1 alone	GLLEKLKEQVTQNFLILECDVKDYGDLPFADIPNDSPFQIVKNPRSVGKASEQLAGKVAEVKKNGRISLVLGGDHSLAIGSISGH ARVHPDLGVIWVDAHTDINTPLTTTSGNLHGQPVSFLLKELKGKIPDVPGFSWVTPCISAKDIVYIGLRDVDPGEHYILKTLGIKY FSMTEVDRLGIGKVMEETLSYLLGRKKRPIHLSFDVDGLDPSFTPATGTPVVGGLTYREGLYITEEIYKTGLLSGLDIMEVNPSL GKTPEEVTRTVNTAVAITLACFGLAREGNHKPIDYLNPPK
Sequence of rhARG1-31 originated by the cleavage of ARG1 by CTSS	~~GLLEKLKE~~QVTQNFLILECDVKDYGDLPFADIPNDSPFQIVKNPSVGKASEQLAGKVAEVKKNGRISLVLGGDHSLAIGSIS HARVHPDLGVIWVDAHTDINTPLTTTSGNLHGQPVSFLLKELKGKIPDVPGFSWVTPCISAKDIVYIGLRDVDPGEHYILKTL GIKYFSMTEVDRLGIGKVMEETLSYLLGRKKRPIHLSFDVDGLDPSFTPATGTPVVGGLTYREGLYITEEIYKTGLLSGLDIME VNPSLGKTPEEVTRTVNTAVAITLACFGLAREGNHKPIDYLNPPK

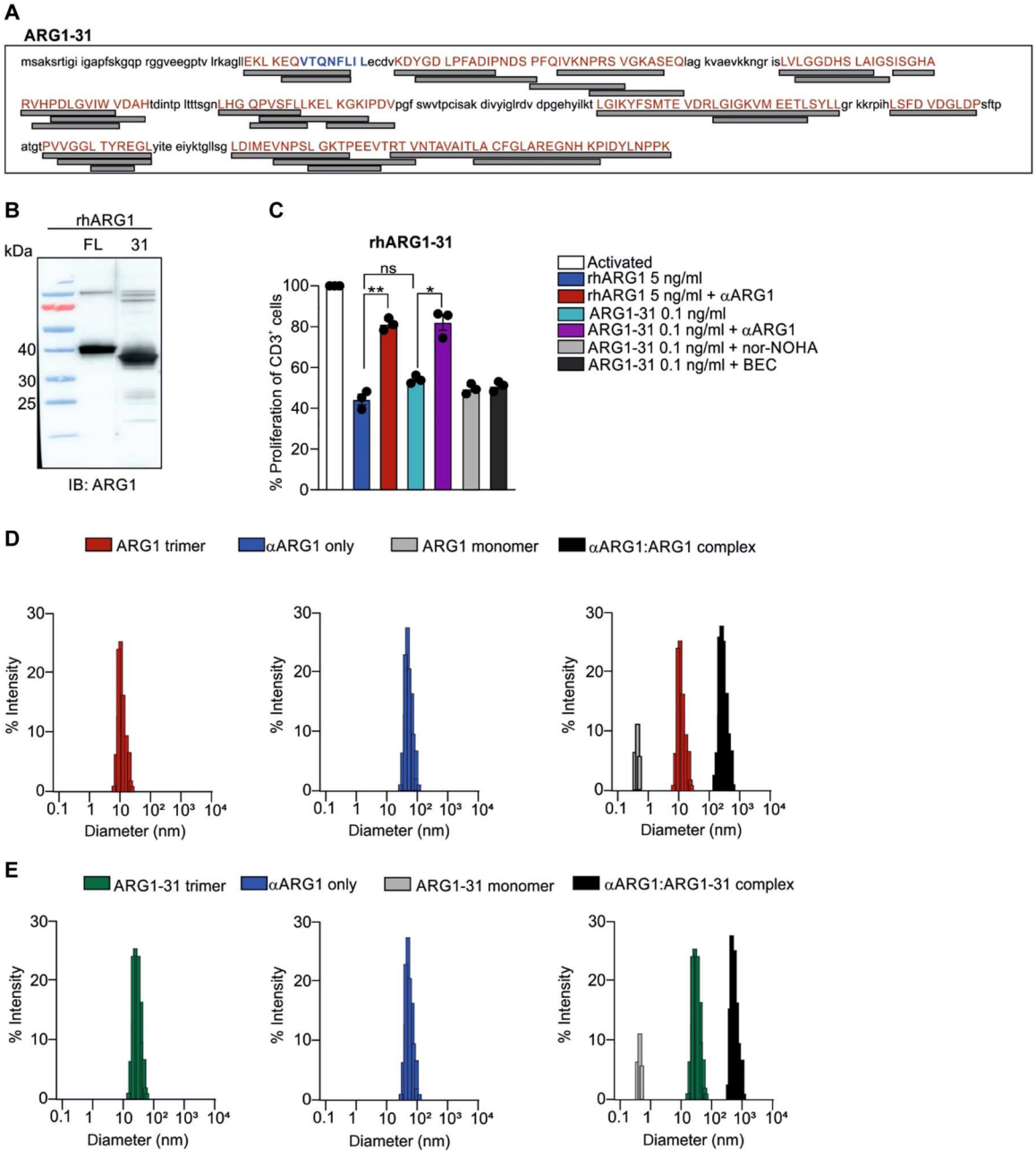

Fig. 3. ARG1's cleaved form has a different enzymatic activity and susceptibility to mAb inhibition. (**A**) Sequence of the ARG1-31 kDa form derived from CTSS-cleaved ARG1 was defined by Mascot analysis. Indicated in red are the peptides identified by the proteomic analysis. The eight amino acids in blue are the unique sequence of the ARG1 isoform 2 (erythroid form) expressed in PMNs. The amino acids in gray represent the ARG1 isoform 2 sequence. (**B**) Immunoblot showing the cloned human ARG1 full-length (ARG1 FL) and ARG1-31 cleaved form. (**C**) Proliferation assay showing the percentage of anti-CD3– and anti-CD28–activated T cells cultured with ARG1 FL or ARG1-31 alone or in combination with different ARG1 inhibitors. Nor-NOHA (30 ng/ml), BEC (10.5 ng/ml), αARG1, and IgG1 control (50 μg/ml) ($n = 3$). Activated T cells were set as 100% proliferation and used as a control. Suppressive activity is represented as the percentage of proliferation of $CD3^+$ $CellTrace^+$ cells. The data are presented as means ± SEM. One-way ANOVA, multiple comparisons, and Tukey's post hoc correction. $^*P < 0.05$; $^{**}P < 0.01$. (**D** and **E**) Dynamic light scattering of (D) full-length rhARG1 (red) and (E) rhARG1-31 (green) alone, Ab clone 1.10 alone (blue), and combination Ab:ARG1 and Ab:ARG1-31 at the ratio of 1:1 (black). Each condition was analyzed in triplicate. A total of two experiments ($N = 2$) were performed with different batches of αARG1 ($n = 3$). Each batch was assessed in triplicate.

Table 5. IC_{50} of full-length ARG1 and cleaved ARG1-31. The table represents the median inhibitory concentration (IC_{50}), defined as the time at which the consumption of L-Arg reaches 50% of the total. Dash indicates that IC_{50} was not reached up to 200 min. BEC, *S*-2-boronoethyl-l-cysteine; nor-NOHA, *N*-hydroxy-nor-L-arginine.

Protein	Time (min)						
	Alone	+αARG1 (ratio 1:1)	+αARG1 (ratio 1:3)	+αARG1 (ratio 1:10)	+αARG1 (ratio 1:30)	+BEC	+nor-NOHA
ARG1-31	11	15	129	-	-	13	10
rhARG1	21	37	48	78	-	-	-

rhARG1-31 share a similar size corresponding to a trimer, whereas monomeric forms were not detected. Therefore, it appears that the trimeric assembly of ARG1 is also maintained by the cleaved form. Next, we evaluated the changes in size of both ARG1 and ARG1-31 upon binding the mAb 1.10, at a molar ratio of 1:1. As shown in Fig. 3 (D and E), the binding of the Ab not only shifted the size of rhARG1 and rhARG1-31 toward a position corresponding to the Ab-protein complex but also produced monomers, suggesting the ability of the Ab clone 1.10 to disrupt the trimeric structure of ARG1. Thus, these findings both underscore the complexity of ARG1 regulation and represent a potential avenue to target ARG1 function.

ARG1 blockade increases the effectiveness of cancer immunotherapy

The dissimilarity between humans and mice regarding the ARG1 cellular source and its species-specific regulation prompted us to establish a humanized mouse model, which allowed the presence of $ARG1^+$ human neutrophils, to test the in vivo efficacy of the αARG1 mAb. In these mice, we exploited either immune checkpoint inhibitors (ICIs) or ACT based on T cells genetically engineered with a T cell receptor (TCR) specific for human telomerase $(hTERT)_{865–873}$ peptide (*54*, *55*). In our previous work (*56*), we showed that $hTERT_{865–873}$-specific $CD8^+$ T cells were not rejected but did not persist in blood of treated mice, as assessed 29 days after adoptive T cell therapy. Moreover, transferred hTERT-specific T cells did not cause graft-versus-host disease and minimally recognized $CD34^+HLA\text{-}A2^+$ cells. Briefly, NOD.Cg-Prkdcscid Il2rgtm1Sug/JicTa (NOG) mice were γ-irradiated and subsequently engrafted with human $HLA\text{-}A2^+CD34^+$ hematopoietic stem cells (*57*). To favor the expansion of neutrophils, we administered recombinant adeno-associated virus serotype 9 vectors (AAV9) coding for human colony-stimulating factor 3, IL-3, IL-8, and hepatocyte growth factor (*58*, *59*) to sustain the systemic release of these cytokines (*60*). Four weeks later, tumor cells were subcutaneously injected. The humanization protocol led to the reconstitution of the major immune cell subsets, such as CD19 B cells, CD3 T cells, CD33 myeloid cells, CD14 monocytes, and CD15 neutrophils (fig. S6, A and B).

To prove the efficacy of the αARG1 clone 1.10, we set up experiments of immunotherapy based on ICI in melanoma (fig. S7A), a tumor that is known to be responsive to immunotherapy. NOG mice were sublethally irradiated and then inoculated with $hCD34^+$ cells, followed by intramuscular injection of cytokine-encoding AAV9. Eight weeks later, SK-MEL-5 melanoma cells were injected subcutaneously. Mounting evidence suggests that a major constraint to ICI includes either the absence of preexisting tumor-specific T cells or their exclusion from the tumor microenvironment. Analyses of pretreatment melanoma biopsies indicated that clinical response to antiprogrammed cell death-1 (PD-1) (*61*) and anticytotoxic T lymphocyte antigen 4 (*62*) correlated with the presence of tumor-infiltrating lymphocytes before the therapy, specifically $CD8^+$ T cells. Nivolumab + ipilimumab (nivo + ipi) reduced the tumor growth, yet the nivo + ipi + αARG1 combination was more effective in controlling cancer progression (fig. S7B), with an impact on mouse survival (Fig. 4A). Moreover, we demonstrated that the nivo + ipi + αARG1 combination therapy increased the percentage of tumor-infiltrating $hCD45^+$ leukocytes (Fig. 4B and fig. S7C) by enhancing the proportion of endogenous activated $hCD3^+$ T cells (Fig. 4, B and C, and fig. S7C). These data suggest that ARG1 blockade in combination with ICI has a therapeutic effect in melanoma by increasing tumor infiltration of activated $CD3^+$ T cells.

These data did not address the issue of whether ARG1 blockade directly affects tumor-specific T cells in humanized mice. For this purpose, we initially assessed SK-MEL-5 cells for their expression of hTERT antigen to exploit the impact of ACT of $hTERT_{865–873}$ TCR-transgenic T cells (*60*). We found that SK-MEL-5 tumor cells expressed hTERT (fig. S7D) and presented hTERT peptide–HLA-A02 complexes on the cell surface, as shown by the interferon-γ (IFN-γ) secretion from cocultured $CD8^+$ T cells (fig. S7, E and F). After the treatment protocol in humanized mice illustrated in fig. S8A, combination therapy (hTERT and αARG1) increased the amount of $CD45^+$ and total $CD3^+$ T cells both in the periphery (fig. S8B) and within the tumor (Fig. 4D and fig. S8C), which also resulted in a higher proportion of tumor infiltration by activated $hTERT_{865–873}$-specific T cells and increased tumor control (Fig. 4D, hTERT, and Fig. 4E). hTERT T cells were identified as positive for the transgene CD34 present in the TCR-expressing lymphocytes, as previously published (*56*). In contrast, the intratumoral myeloid compartment remained unmodified with treatment (Fig. 4F and fig. S8C). Furthermore, SK-MEL-5 tumors established in humanized mice were infiltrated with human $CD66b^+$ neutrophils (fig. S9A) expressing ARG1 and were enriched in NETs (fig. S9, B to D) presenting reactivity to both hARG1 (fig. S9, B, C, and E) and hCTSS (fig. S9, B, C, and F) that colocalized (fig. S9G). When we evaluated the functional features of hTERT-specific T cells isolated from SK-MEL-5 tumors, we found that T cells had a higher proliferation capacity as well as higher expression of CD69 and CD25, but not PD-1, suggesting a shift toward activation in mice treated with the combination therapy (Fig. 4G and fig. S8C). Thus, in vivo ARG1 blockade can improve the effectiveness of cancer immunotherapy by sustaining the functional activity of tumor-infiltrating T cells.

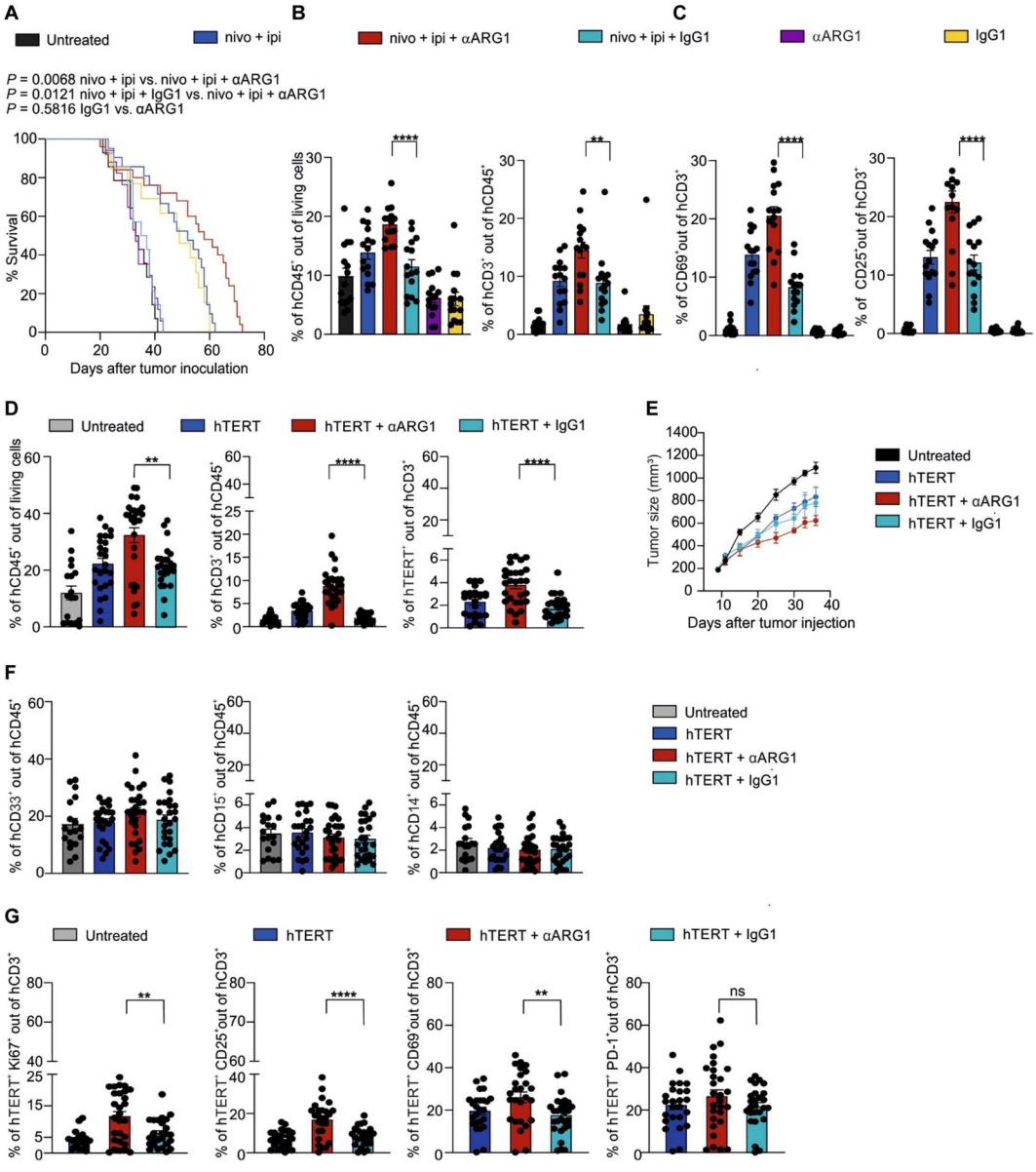

Fig. 4. ARG1 blockade increases the effectiveness of cancer immunotherapy. (**A**) Kaplan-Meier plots evaluating the survival of SK-MEL-5–bearing humanized mice ($N = 2$). The data are presented as percentage of survival. Treatment was started 13 days after tumor injection. Untreated ($n = 29$), nivo + ipi ($n = 36$), nivo + ipi + αARG1 ($n = 35$), nivo + ipi + IgG1 ($n = 33$), IgG1 ($n = 29$), and αARG1 ($n = 35$). Log-rank test; nivo + ipi versus nivo + ipi + αARG1, $^{**}P = 0.0068$; nivo + ipi + IgG1 versus nivo + ipi + αARG1, $^{*}P = 0.0121$; IgG1 versus αARG1, not significant, $P = 0.5816$. (**B** and **C**) Quantified FACS analysis evaluating the percentages of tumor-infiltrating human immune cells in mice bearing SK-MEL-5 tumors ($N = 2$). Humanized mice were treated with nivo + ipi ($n = 15$), nivo + ipi + αARG1 ($n = 15$), nivo + ipi + IgG1 ($n = 15$), αARG1 ($n = 15$) alone, IgG1 ($n = 15$) alone, or left untreated. Mice were euthanized at 30 days after tumor inoculation. Cells were defined on the basis of the expression of hCD45 (B, left), hCD3 (B, right), hCD69 (C, left), and hCD25 (C, right). The data are represented as means ± SEM. One-way ANOVA, multiple comparisons, and Tukey's post hoc correction. $^{**}P = 0.0097$; $^{****}P < 0.0001$. (**D**) Quantified FACS analysis evaluating the percentages of tumor-infiltrating human immune cells in mice bearing SK-MEL-5 tumors ($N = 2$). Treatment was started 11 days after tumor injection. Humanized mice were treated with $hTERT_{865–873}$ TCR-transgenic $CD8^+$ T alone ($n = 26$) or in combination with neutralizing αARG1 ($n = 28$), IgG1 isotype control ($n = 26$), or left untreated ($n = 20$). Cells were defined on the basis of the expression of hCD45, hCD3, and hCD34 marker that defines $hTERT_{865–873}$-specific T cells. The data are presented as means ± SEM. One-way ANOVA, multiple comparisons, and Tukey's post hoc correction. $^{**}P = 0.0046$; $^{****}P < 0.0001$. (**E**) Determination of the tumor size (volume, mm^3), in SK-MEL-5 tumor model, injected subcutaneously in humanized mice ($N = 2$). Cumulative tumor size curves of the different treatment groups are shown; untreated ($n = 27$), hTERT ($n = 30$), hTERT + αARG1 ($n = 30$), hTERT + IgG1 ($n = 24$). The data are presented as mean ± SD. Two-way ANOVA, multiple comparisons, and Tukey's post hoc correction. Untreated versus hTERT, $^{****}P < 0.0001$; hTERT + αARG1 versus hTERT + IgG1, $^{**}P = 0.00256$. (**F**) Quantified FACS analysis evaluating the percentages of tumor-infiltrating human immune cells in mice bearing SK-MEL-5 tumors ($N = 2$) treated as in (D). Myeloid cells, defined on the basis of the expression of hCD33, hCD15, and hCD14, are shown. The data are presented as mean ± SEM. (**G**) Quantified FACS analysis of $hCD3^+hCD34^+$ $hTERT_{865–873}$ TCR-transgenic $CD8^+$ T cells, isolated from SK-MEL-5 tumors ($N = 2$), evaluating the expression of proliferation (Ki-67) and activation (CD25, CD69, and PD-1) markers. $hTERT_{865–873}$ transgenic $CD8^+$ T cells were isolated from mice treated with $hTERT_{865–873}$ TCR-transgenic $CD8^+$ T cells alone ($n = 26$) or in combination with neutralizing αARG1 ($n = 28$) or IgG1 isotype control ($n = 26$) or left untreated ($n = 20$). The data are presented as means ± SEM. One-way ANOVA, multiple comparisons, and Tukey's post hoc correction. $^{**}P = 0.0091$ and $^{****}P < 0.0001$.

Neutralization of ARG1 increases the proportion and functional status of tumor-infiltrating lymphocytes

We next assessed whether ARG1 blockade increases the infiltration and fitness of adoptively transferred $hTERT_{865–873}$ TCR-transgenic T cells in a humanized mouse model of PDAC known to be refractory to immunotherapy. Similar to SK-MEL-5, PT-45 cells expressed hTERT (fig. S7D) and presented hTERT peptide–HLA-A02 complexes on the cell surface, as shown by the IFN-γ secretion by $hTERT_{865–873}$ TCR-transgenic T cells (fig. S7, E and F). PT-45 tumor–bearing mice were treated as previously indicated (fig. S8A). ARG1 blockade in combination with ACT increased the total amount of blood and tumor-infiltrating leukocytes, specifically

$CD3^+$ T lymphocytes (Fig. 5A and fig. S10, A and B). Among the latter, hTERT-specific T cells also expanded (Fig. 5A and fig. S10B, hTERT), leading to better tumor control (Fig. 5B) and an unaltered myeloid compartment (Fig. 5C and fig. S10B). In addition, ARG1 blockade enhanced the expression of proliferation and activation markers in adoptively transferred $hTERT^+$ $CD8^+$ T cells (Fig. 5D and fig. S10B), demonstrating the ability of this treatment to reprogram the immunosuppressive microenvironment of PDAC.

To evaluate the efficacy of nivo + ipi + anti-ARG1 combination treatment, we set up an ex vivo protocol using resected PDAC tumors from treatment-naïve patients. Tumors were mechanically digested, debris were removed, and the tumor cellular framework was evaluated by fluorescence-activated cell sorting (FACS) analysis for CD45, CD3, CD8, and CD66b markers. Purified $CD45^+$ cells were incubated with nivo + ipi and αARG1, either alone or in combination (fig. S11A) (*63*). As shown in Fig. 5E, the nivo +

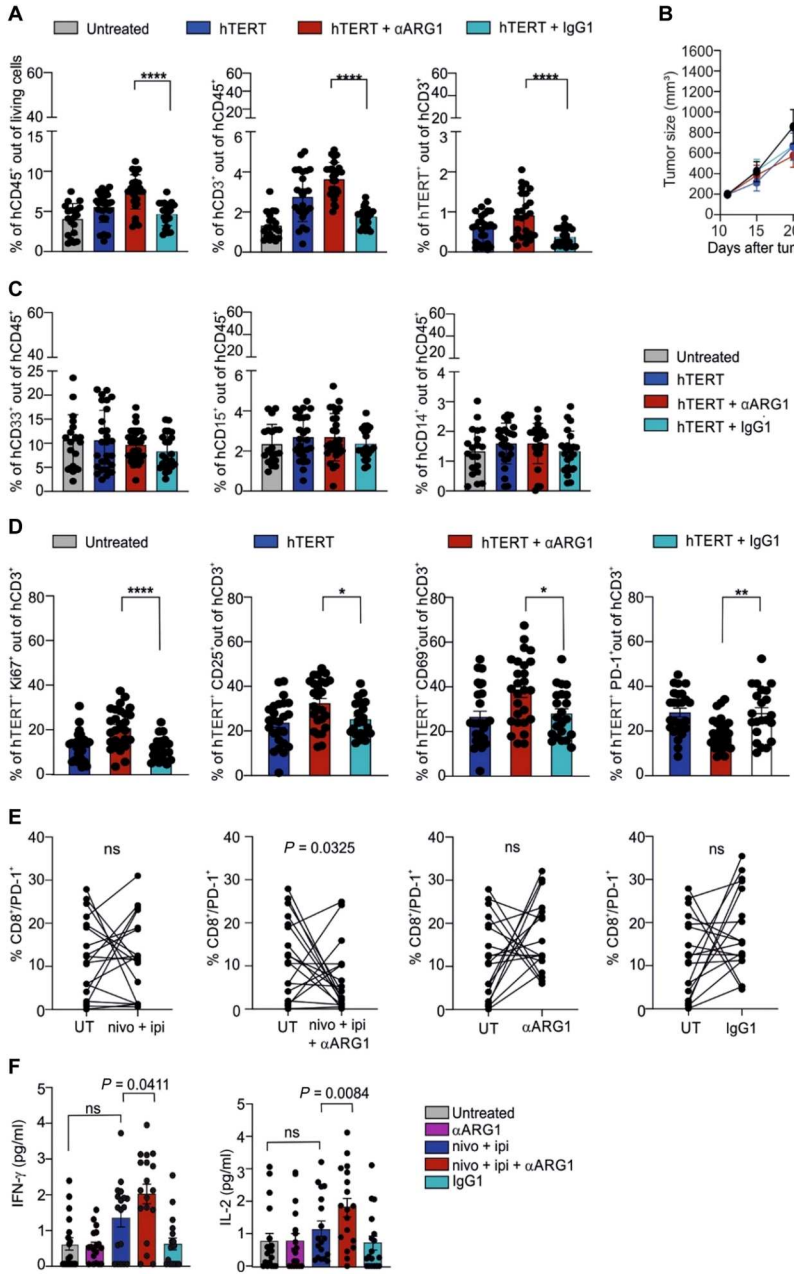

Fig. 5. Neutralization of ARG1 increases the proportion and functional status of tumor-infiltrating lymphocytes when combined with immunotherapy. (**A**) Quantified FACS analysis evaluating the percentages of tumor-infiltrating human immune cells in mice bearing subcutaneous PT-45 tumors ($N = 2$). Humanized mice were treated with $hTERT_{865–873}$ TCR-transgenic $CD8^+$ T cells alone ($n = 26$) or in combination with neutralizing αARG1 ($n = 28$) or IgG1 isotype control ($n = 26$). Human immune cells were defined on the basis of the expression of hCD45 and hCD3; hTERT TCR-transgenic $CD8^+$ T cells were defined on the basis of the expression of the CD34 marker. The data are presented as means ± SEM. One-way ANOVA, multiple comparisons, and Tukey's post hoc correction. $^{****}P < 0.0001$. (**B**) Determination of the tumor size (volume, mm^3), in PT-45 tumor model, injected subcutaneously in humanized mice ($N = 2$). Cumulative tumor size curves of the different treatment groups are shown; untreated ($n = 23$), hTERT ($n = 28$), hTERT + αARG1 ($n = 30$), and hTERT + IgG1 ($n = 25$). The data are presented as means ± SD. Two-way ANOVA, multiple comparisons, and Tukey's post hoc correction. Untreated versus hTERT, $^{****}P < 0.0001$; hTERT + αARG1 versus hTERT + IgG1, $^{****}P < 0.0001$. (**C**) Quantified FACS analysis evaluating the percentages of tumor-infiltrating human immune cells in mice bearing SK-MEL-5 tumors ($N = 2$) treated as in (A). Myeloid cells, defined on the basis of the expression of hCD33, hCD15, and hCD14, are shown. The data are presented as means ± SEM. (**D**) Quantified FACS analysis of hCD3 + hCD34+ hTERT–specific T cells, isolated from PT-45 tumors ($N = 2$), evaluating the expression of proliferation (Ki-67) and activation (CD25, CD69, and PD-1) markers. hTERT-transgenic T cells were isolated from PT-45 tumors of mice treated with hTERT865–873 TCR-transgenic CD8+ T cells alone ($n = 26$) or in combination with neutralizing αARG1 ($n = 28$) or IgG1 isotype control ($n = 26$). The data are presented as means ± SEM. One-way ANOVA, multiple comparisons, and Tukey's post hoc correction. $^*P = 0.0292$, $^{**}P = 0.0028$, and $^{****}P = 0.0001$. (**E**) Quantified FACS analysis of $CD8^+PD\text{-}1^+$ cells in tumor tissue homogenates ex vivo, derived from naïve-treatment patients with PDAC ($n = 21$), cultured for 24 hours with either nivo + ipi, nivo + ipi + αARG1, αARG1, isotype IgG1 control, or left untreated. The data are presented as means ± SEM. Paired, two-tailed, Student's *t* test. (**F**) Quantification by ELISA of IFN-γ and IL-2 secreted in the SNs of cells treated for 24 hours as in (C). The data are presented as means ± SEM. One-way ANOVA, multiple comparisons, and Tukey's post hoc correction.

ipi + αARG1 treatment resulted in a decrease in the amount of $CD8^+$ T cells expressing PD-1, which was paralleled by an increase in IFN-γ and IL-2 release (Fig. 5F). These effects were independent of the percentage of leucocyte subsets because these subsets were unaltered among the various treatment groups (fig. S11B). These data suggest that harnessing ARG1 activity in PDAC might enhance the efficacy of nivo + ipi therapy, currently confined to a minority of patients (*6*).

DISCUSSION

Tumors have long been known to consume glucose and other nutrients to grow and proliferate (*64*), making their microenvironment metabolically deprived and restrictive for infiltrating immune cells. This is true particularly for antitumor-specific T cells, which necessitate L-Arg to sustain their activation and functions (*19*, *65*). In humans, PMNs are the main source of ARG1, one of the few amino acid–metabolizing enzymes whose activity is linked to the control of immune responses (*66*). Profound differences in the ARG1 biology and compartmentalization between humans and rodents raised questions of whether the two analogs act similarly and how the enzyme can efficiently work in the extracellular environment at pH 7.4. hARG1, freed upon PMN cell death, was shown to suppress natural killer cell proliferation (*67*). However, the fate of ARG1 upon PMN degranulation and its impact on restraining human antitumor T cell response are still unknown. Degranulation involves the fusion of granules with the plasma membrane and the release of factors into the extracellular space. The tertiary granules, where ARG1 resides, lack the soluble *N*-ethylmaleimide–sensitive factor attachment protein receptors that would direct them to fuse with the plasma membrane (*68*). Therefore, the content of these granules is either deployed inside the phagosome or released extracellularly through the formation of NETs. Confocal analysis of activated PMNs revealed a controlled release of granules′ ARG1 that in part localized along the ordered web-like stranded chromatin. We demonstrated that ARG1 in NETs is endowed with an enzymatic proficiency at physiological pH, which we assessed in terms of both downstream ornithine production and immunosuppressive activity toward activated T cells. We also addressed the mechanisms controlling enzymatic activation and identified a biochemical pathway in NET-associated ARG1. Our findings support a scenario in which NETs form stable, enzymatically active aggregates precluding the spread of these enzymes into surrounding normal tissue but allowing them to affect the concentration of nutrients, metabolites, and other mediators. ARG1 in NETs could rapidly decrease the local concentrations of L-Arg to a threshold sufficient to arrest effector T cell functions, similarly to an antimicrobial response. The mechanistic foundation for the enzyme cleavage and activation relies on the close physical interaction between CTSS and ARG1. The appearance of ARG1 high–molecular weight bands at late time points of NET assembly suggests a situation in which products of the cleavage or uncut full-length protein assemble into molecular complexes that are thermodynamically favored and stable, as suggested by the higher catalytic activity.

Recent studies have suggested that NETs are associated with cancer cell awakening and metastatic spread in mouse models (*33*, *69*). However, the NET presence in human cancers, their role, contribution to treatment response, and efficacy remain largely unknown. Because of hARG1′s unique species-specific biology, it is necessary to reconsider its targeting and better investigate the findings from current inhibitors. We showed that classical ARG1 inhibitors have no effect on the cleaved form of ARG1, which was in contrast to hARG1 mAbs. Although small-molecule ARG1 inhibitors are being tested in phase 1 clinical trials, several issues argue that this approach might be biased because of the majority of experiments being performed preclinically in mouse models. As a side effect, small-molecule inhibitors can affect the urea cycle in the liver, causing hyperammonemia, with unpredictable results on the overall antitumor immune response. Moreover, as shown in this manuscript, the current ARG1 inhibitors are not active on hARG1-cleaved forms or high–molecular weight complexes derived from them. The simple explanation is that they were designed and synthesized on the basis of the knowledge acquired, over several decades, on the full-length enzyme. In this scenario, the availability of cleaved forms might offer a simple in vitro substrate to screen and identify novel, effective, and specific inhibitors.

Ab-based therapeutics against cancer are highly successful in the clinic and currently enjoy unprecedented recognition for their potential. Current Ab drugs have fewer adverse effects because of their high specificity. As a result, therapeutic Abs have emerged as the predominant class of new drugs developed in recent years. In this regard, targeting hARG1 using a neutralizing Ab acting on extracellular and active forms of hARG1 is expected to be effective and safer than a total inhibition of arginases by small molecules. Our mAb was shown to be specific for the hARG1 isoform, with a high binding affinity, and was capable of neutralizing ARG1 activity in a dose-dependent manner. Moreover, our data suggest that the mAb clone 1.10 recognizes, binds, and neutralizes not only the full-length but also the ARG1 cleaved forms, indicating a broader effect on ARG1-mediated immunosuppression. In humanized mouse models of cancers, which represent models of either immunotherapy responsiveness, such as SK-MEL-5 melanoma, or resistance, such as PT-45 PDAC, we found that ARG1 neutralization in combination with ACT enhanced the persistence of tumor-specific T cells inside the tumor and boosted their functional activity. These data could help pave the way to translation of the combination therapy to the clinic, as indicated by the efficacy of αARG1 and nivo + ipi.

There are limitations to this study, and further work is needed before a first-in-human clinical trial. First, fully human mAbs to hARG1 are needed. Second, we cannot specifically detect the ARG1 cleaved forms in the sera of patients with PDAC. The absence of Abs specifically recognizing hARG1 cleaved forms limits the ability to understand their contribution to immunosuppression and target them for combination immunotherapy. However, the ARG1 enzyme activity at pH 7.4 is increased in those with PDAC compared with HDs. Because this increase is linked to the presence of cleaved forms, we can reasonably argue that ARG1 is cleaved and circulating in the patients′ sera. Moreover, we do not have evidence to claim unequivocally that CTSS cleaves ARG1 in PDAC sera. These issues will be addressed in future experiments. Third, the reconstitution of the human immune system with engrafted $CD34^+$ human precursors in NOG mice is far from being complete. The presence of defective key lymphoid organs, like the thymus and the spleen, negatively affects the overall repertoire of human endogenous T cell clones and their affinity. The lack of these functional organs could explain why it is

difficult to observe enduring tumor regression, as seen in inbred immunocompetent mice.

Improvement in treatments for patients with PDAC is urgent, because they have a very dismal prognosis. PDAC tumors show a remarkable resistance to immunotherapy, including vaccination, adoptive T cell therapy, and immune checkpoint blockade. This likely reflects multiple mechanisms, among which a TME heavily infiltrated by immunosuppressive cells and a dense stroma are the most relevant. Neutrophils and macrophages are the most abundant immune cell type within the TME and are associated with poor clinical prognosis because of their immunosuppressive properties and roles in sustaining therapeutic resistance. Whereas different strategies have been set and are currently being investigated in clinical trials, a limited number of therapies targeting neutrophils, both as a number and as a function, have been developed so far. Here, we showed that LDNs and NDNs from patients release NETs as a result of their constitutive activation that might be contributed by the high serum levels of IL-8 and TNF-α. Furthermore, recent findings implicated high IL-8 as correlated with poor outcome in patients with cancer and reduced clinical benefits of ICI-based therapy (*49*). In NETs, we found that ARG1 is present in different molecular forms that contribute to ARG1 gain of function at physiological pH. The presence of ARG1 active in the blood at physiological pH might be a marker for patients′ stratification and prognosis during disease follow-up. Our studies also support the option to block CTSS with an antagonistic Ab, especially in tumors where this enzyme is present at higher amounts like colorectal carcinomas (*70*). In conclusion, our data describe a novel pathway to generate hARG1 active forms whose negative impact on the immune response can be targeted by αARG1 mAb. These findings support the use of αARG1 mAbs, in combination with immunotherapy, as potential treatment for PDAC and warranting further exploration in patients with solid cancer.

MATERIALS AND METHODS

Study design

The overall objectives were to define human ARG1 biology, its mechanisms of action in human neutrophils and NETs, and its role in driving the immunosuppression in patients with PDAC cancer and to develop a targeting strategy and assess the efficacy of such therapy in combination with immunotherapy in humanized mouse models of melanoma and PDAC. The clinical characteristics and the numbers of the patients and HDs are listed in Table 1. Patients′ eligibility criteria are indicated in Materials and Methods. Patients′ selection was not randomized or blinded. Blood samples were processed immediately to isolate neutrophils. Neutrophils and NETs were evaluated by flow cytometry, proteomic, biochemical, and imaging assays. Tumor tissues from patients with PDAC were collected upon written informed consent and mechanically digested upon receipt. $CD45^+$ cells were isolated, cultured with specific Abs, and analyzed by flow cytometry and enzyme-linked immunosorbent assay (ELISA).

NOG mice were sublethally irradiated and engrafted with human $CD34^+$ cells. Mice with a humanization amount of or above 25 to 30% engraftment were randomly distributed among the different experimental groups. All analyses were performed in a blinded manner with regard to treatment. Mice were treated as here in Material and Methods. To estimate the sample size, we followed several parameters such as size effect, variability, and power. The experiments were performed twice. For each in vivo animal studies, we performed pilot studies to define the feasibility and determine the number of animals required per group in order to observe an effect.

Human samples

PB samples, tumor tissues, and sera were collected from patients with stages III and IV PDAC, admitted at the Unit of General and Pancreatic Surgery of the Azienda Ospedaliera Universitaria Integrata of Verona before surgical resection, or HDs. Clinical pathologic features of patients and HD are reported in Table 1. No patient had a prior history of cancer or was undergoing therapy at the time of sample collection. All patients were over 18 years old.

Informed consent was obtained from all participants, and the study was approved by the Ethics Committee: for the use of PDAC and HD PBMCs, Prot. 25978, Prog. 2172 on 29 May 2012 principal investigator A. Scarpa; for the use of PBMCs isolated from buffy coats or PB of HDs Prot. 24114 on 16 May 2017 principal investigator V. Bronte.

Isolation of human PBMCs and PMNs

PB from patients with PDAC was collected in EDTA-coated tubes and layered on top of Ficoll-Paque plus (17-1440-03, GE Healthcare) to obtain the PBMC and red blood cell (RBC) fractions. Upon stratification, cells were spun at 400*g* for 30 min at room temperature, and brake was turned off. The PBMC fraction was collected, washed three times with phosphate-buffered saline (PBS), and then cells were counted. LDNs were isolated from PBMCs by the sequential addition of CD66b–fluorescein isothiocyanate (FITC) Ab (555724, BD Biosciences) and microbeads anti-FITC (130-048-701, Miltenyi Biotec) following the manufacturer′s instructions. NDNs were isolated from the RBC layer by dextran density gradient (31392, Sigma-Aldrich), and after 20-min incubation at 25°C, the upper layer was collected. The cells were spun at 200*g* for 5 min at 25°C, and then the remaining contaminant RBCs were lysed with 4 ml of 0.2% NaCl solution (30 s, 25°C), followed by the addition of 9 ml of 1.2% of NaCl solution. PMNs from HDs were plated and stimulated with ionomycin calcium salt (5 μM; 10634-5MG, Sigma-Aldrich) for 30 min or 2 hours. At the end of the stimulation, NET-enriched SNs and cells were collected and used for downstream assays. The NDNs were isolated by CD66b-Ab as LDNs. Isolated cells from patients with PDAC were plated for 12 hours without stimulation, and then NET-enriched SNs, SNs containing free ARG1, and cells were collected and used for downstream assays. Samples with purity, evaluated by FACS analysis, greater than 95% were assessed in the functional assay.

Mice

NOG mice and Balb/c mice were purchased from Taconic Biosciences. All mice were maintained under specific pathogen–free conditions in the animal facility of the University of Verona. Animal experiments were performed according to national (protocol number 12722 approved by the Ministerial Decree Number 14/2012-B of 18 January 2012 and protocol number BR15/08 approved by the Ministerial Decree Number 925/2015-PR of 28 August 2015) and European laws and regulations. All animal experiments were approved by Verona University Ethical Committee (https://univr.it/it/cirsal) and conducted according to the guidelines of Federation

of European Laboratory Animal Science Association. In each animal experiment, both sexes were used, and mice were randomly assigned to each group. For the humanization experiments, NOG mice older than 4 weeks were not eligible for receiving $hCD34^+$ cells (exclusion criteria).

Systemic treatment of humanized mice with $hTERT_{865–873}$ TCR–engineered T cells

Ten weeks after AAV9 transfer, human immune–reconstituted (HIR) mice were inoculated subcutaneously with 10^6 SK-MEL-5 or PT-45 cell lines. When the tumor reached 200 mm^3, the treatments started [V (mm^3) = (d2 x D)/2, where d (mm) and D (mm) are the smallest and largest perpendicular tumor diameters, respectively, as assessed by caliper measurement]. $hTERT_{865–873}$ TCR–engineered T cells (2.5×10^6) were injected intravenously every 5 days for the first two injections and then once a week for the last two injections. The Ab αARG1 clone 1.10 followed the same scheme of injection of $hTERT_{865–873}$ TCR–engineered T cells except that it was administered 2 days in advance. The mAb generation is described in the Supplementary Materials and Methods and includes figs. S12 and S13 and tables S1 to S3. At the same time of the adoptive T cell transfer, IL-2 (20 IU/ml) was injected intraperitoneally (Novartis), and then IL-2 was given every other day. The day before $hTERT_{865–873}$ TCR–engineered T cell injection, the mice received αARG1 clone 1.10 or IgG1 isotype control (20 mg/kg) intraperitoneally. Two days after the last $hTERT_{865–873}$ TCR–engineered T cell injection, the mice were euthanized, and organs (spleen, lymph nodes, tumor, and bone marrow) were collected and analyzed by flow cytometry and IF. Some mice received $hTERT_{865–873}$TCR–engineered T cells only or in combination with αARG1 clone 1.10 or IgG1 isotype control. Some mice were left untreated.

Systemic treatment of humanized mice with checkpoint inhibitors

HIR mice were inoculated at week 8 from $CD34^+$ engraftment, with 10^6 SK-MEL-5 melanoma cells. When the tumor reached 200 mm^3, some mice received a combination of nivolumab (10 mg/kg ip; Opdivo, Bristol Mayers Squibb) and ipilimumab (5 mg/kg ip; Yervoy, Bristol Mayers Squibb) every 5 days [doses and schedule were adapted from (*71*)]. Some mice received αARG1 clone 1.10 (20 mg/kg) intraperitoneally alone or in combination with nivolumab and ipilimumab.

Proliferation assay

For samples derived from HDs, 5×10^5 PMNs resuspended in L-Arg–free complete RPMI 1640 (06-1100-07-1A, Biological Industries) were seeded in 24-well plates, and they were stimulated with ionomycin calcium salt (5 μM; 10634-5MG, Sigma-Aldrich) for 30 min or 2 hours, and at the end of the stimulation, NET-enriched SNs were collected. Alternatively, from PDAC-derived samples, 2×10^5 to 5×10^5 NDN $CD66b^+$ or LDN $CD66b^+$, resuspended in L-Arg–free complete RPMI, were seeded in 24-well plates, and after 12 hours, NET-enriched SNs were collected. CellTrace-labeled PBMCs (4×10^4 to 8×10^4) were resuspended in the appropriate NET-enriched SNs according to the experiment and were stimulated with coated anti-CD3 (clone: OKT-3, 16-0037-81, Thermo Fisher Scientific) and soluble anti-CD28 (clone: CD28.2, 16-0289-81, Thermo Fisher Scientific). One hundred fifty micromolar L-Arg (Sigma-Aldrich) was also added in the culture. According to each experiment, inhibitors or Abs were added: αARG1 clone 1.10, isotype IgG1 (150 μg/ml), nor-NOHA (30 ng/ml; 399275, Calbiochem), BEC (10.5 ng/ml; 197900, Calbiochem), and rhARG1 (5 ng/ml). For the PDAC samples, the functional assay was performed by adding 200 μl of serum instead of L-Arg–free complete RPMI. As positive control, we used PMBCs stimulated with bound anti-CD3 and soluble anti-CD28 Abs. As negative control, we used (resting) PBMCs in RPMI L-Arg–free media, in which we added 150 μM L-Arg. At the end of the culture, cells were stained with anti–CD3-phycoerythrin-cyanine 7 (clone: UCHT1, 25-0038-42, Thermo Fisher Scientific), proliferating T cells were acquired, and data were analyzed with FlowJo Software (Tree Star Inc., Ashland).

NET formation and quantification

NETs were isolated from neutrophils derived both from patients with PDAC and HDs. PMNs were plated at 1×10^6/ml, and PMNs derived from HDs were stimulated with ionomycin calcium salt (5 μM; 10634, Sigma-Aldrich) for 30 min or 2 hours at 37°C. At the end of the stimulation, NET-enriched SNs were collected. Briefly, SN was removed and kept for analysis and NETs adhered at the bottom of the plate were detached and centrifuged at 1000*g* at 4°C for 10 min. The cell-free SN containing NETs (DNA-protein complex) was collected. DNA content was quantified using NanoDrop ONE (13400518, Thermo Fisher Scientific). Pelleted cells were washed with 2 mM PBS-EDTA and used in some experiments.

NET quantification by DNA-MPO complex ELISA

NETs were quantified following the protocol published by Veras *et al.* (*72*). Briefly, 96-well plates were coated with the anti-MPO Ab (PA5-16672, Thermo Fisher Scientific) overnight at 4°C and then blocked with 1% bovine serum albumin. Samples containing NETs were incubated for 2 hours at 25°C with gentle shaking (320 rpm). The complex of DNA-MPO was quantified with the Quant-iT PicoGreen kit (P11496, Thermo Fisher Scientific) according to the manufacturer's instructions.

Statistical analyses

Statistical analyses were performed using GraphPad Prism 8 (GraphPad Software). The data are presented either as mean ± SEM or mean ± SD. Statistical comparisons were performed using two-way analysis of variance (ANOVA), one-way ANOVA, Student's t test, and log-rank test. Tukey's post hoc correction method was used when multiple comparisons were performed. $P < 0.05$ was considered statistically significant. Parametric tests were used upon normality check. GraphPad uses the traditional $\alpha = 0.05$ cutoff to answer the question of whether the data passed the normality test.

Supplementary Materials

This PDF file includes:
Materials and Methods
Figs. S1 to S13
Tables S1 to S3

Other Supplementary Material for this manuscript includes the following:
Data files S1 and S2
MDAR Reproducibility Checklist

View/request a protocol for this paper from *Bio-protocol*.

REFERENCES AND NOTES

1. R. L. Siegel, K. D. Miller, H. E. Fuchs, A. Jemal, Cancer statistics, 2021. *CA Cancer J. Clin.* **71**, 7–33 (2021).
2. I. Garrido-Laguna, M. Hidalgo, Pancreatic cancer: From state-of-the-art treatments to promising novel therapies. *Nat. Rev. Clin. Oncol.* **12**, 319–334 (2015).
3. T. Conroy, P. Hammel, M. Hebbar, M. B. Abdelghani, A. C. Wei, J. L. Raoul, L. Chone, E. Francois, P. Artru, J. J. Biagi, T. Lecomte, E. Assenat, R. Faroux, M. Ychou, J. Volet, A. Sauvanet, G. Breysacher, F. Di Fiore, C. Cripps, P. Kavan, P. Texereau, K. Bouhier-Leporrier, F. Khemissa-Akouz, J. L. Legoux, B. Juzyna, S. Gourgou, C. J. O'Callaghan, C. Jouffroy-Zeller, P. Rat, D. Malka, F. Castan, J. B. Bachet; Canadian Cancer Trials Group and the Unicancer-GI–PRODIGE Group, FOLFIRINOX or gemcitabine as adjuvant therapy for pancreatic cancer. *N. Engl. J. Med.* **379**, 2395–2406 (2018).
4. T. Conroy, F. Desseigne, M. Ychou, O. Bouche, R. Guimbaud, Y. Becouarn, A. Adenis, J. L. Raoul, S. Gourgou-Bourgade, C. de la Fouchardiere, J. Bennouna, J. B. Bachet, F. Khemissa-Akouz, D. Pere-Verge, C. Delbaldo, E. Assenat, B. Chauffert, P. Michel, C. Montoto-Grillot, M. Ducreux; Groupe Tumeurs Digestives of Unicancer; PRODIGE Intergroup, FOLFIRINOX versus gemcitabine for metastatic pancreatic cancer. *N. Engl. J. Med.* **364**, 1817–1825 (2011).
5. A. H. Morrison, K. T. Byrne, R. H. Vonderheide, Immunotherapy and prevention of pancreatic cancer. *Trends Cancer* **4**, 418–428 (2018).
6. D. T. Le, J. N. Durham, K. N. Smith, H. Wang, B. R. Bartlett, L. K. Aulakh, S. Lu, H. Kemberling, C. Wilt, B. S. Luber, F. Wong, N. S. Azad, A. A. Rucki, D. Laheru, R. Donehower, A. Zaheer, G. A. Fisher, T. S. Crocenzi, J. J. Lee, T. F. Greten, A. G. Duffy, K. K. Ciombor, A. D. Eyring, B. H. Lam, A. Joe, S. P. Kang, M. Holdhoff, L. Danilova, L. Cope, C. Meyer, S. Zhou, R. M. Goldberg, D. K. Armstrong, K. M. Bever, A. N. Fader, J. Taube, F. Housseau, D. Spetzler, N. Xiao, D. M. Pardoll, N. Papadopoulos, K. W. Kinzler, J. R. Eshleman, B. Vogelstein, R. A. Anders, L. A. Diaz Jr., Mismatch repair deficiency predicts response of solid tumors to PD-1 blockade. *Science* **357**, 409–413 (2017).
7. E. Karamitopoulou, Tumour microenvironment of pancreatic cancer: Immune landscape is dictated by molecular and histopathological features. *Br. J. Cancer* **121**, 5–14 (2019).
8. J. W. Hickey, Y. Tan, G. P. Nolan, Y. Goltsev, Strategies for accurate cell type identification in CODEX multiplexed imaging data. *Front. Immunol.* **12**, 727626 (2021).
9. J. R. Lin, B. Izar, S. Wang, C. Yapp, S. Mei, P. M. Shah, S. Santagata, P. K. Sorger, Highly multiplexed immunofluorescence imaging of human tissues and tumors using t-CyCIF and conventional optical microscopes. *eLife* **7**, e31657 (2018).
10. J. L. Carstens, P. Correa de Sampaio, D. Yang, S. Barua, H. Wang, A. Rao, J. P. Allison, V. S. LeBleu, R. Kalluri, Spatial computation of intratumoral T cells correlates with survival of patients with pancreatic cancer. *Nat. Commun.* **8**, 15095 (2017).
11. I. M. Stromnes, A. Hulbert, R. H. Pierce, P. D. Greenberg, S. R. Hingorani, T-cell Localization, activation, and clonal expansion in human pancreatic ductal adenocarcinoma. *Cancer Immunol. Res.* **5**, 978–991 (2017).
12. S. A. Vayrynen, J. Zhang, C. Yuan, J. P. Vayrynen, A. D. Costa, H. Williams, V. Morales-Oyarvide, M. C. Lau, D. A. Rubinson, R. F. Dunne, M. M. Kozak, W. Wang, D. Agostini-Vulaj, M. G. Drage, L. Brais, E. Reilly, O. Rahma, T. Clancy, J. Wang, D. C. Linehan, A. J. Aguirre, C. S. Fuchs, L. M. Coussens, D. T. Chang, A. C. Koong, A. F. Hezel, S. Ogino, J. A. Nowak, B. M. Wolpin, Composition, Spatial characteristics, and prognostic significance of myeloid cell infiltration in pancreatic cancer. *Clin. Cancer Res.* **27**, 1069–1081 (2021).
13. C. Tian, D. Ohlund, S. Rickelt, T. Lidstrom, Y. Huang, L. Hao, R. T. Zhao, O. Franklin, S. N. Bhatia, D. A. Tuveson, R. O. Hynes, Cancer cell-derived matrisome proteins promote metastasis in pancreatic ductal adenocarcinoma. *Cancer Res.* **80**, 1461–1474 (2020).
14. C. Tian, K. R. Clauser, D. Ohlund, S. Rickelt, Y. Huang, M. Gupta, D. R. Mani, S. A. Carr, D. A. Tuveson, R. O. Hynes, Proteomic analyses of ECM during pancreatic ductal adenocarcinoma progression reveal different contributions by tumor and stromal cells. *Proc. Natl. Acad. Sci. U.S.A.* **116**, 19609–19618 (2019).
15. M. Sano, H. Ijichi, R. Takahashi, K. Miyabayashi, H. Fujiwara, T. Yamada, H. Kato, T. Nakatsuka, Y. Tanaka, K. Tateishi, Y. Morishita, H. L. Moses, H. Isayama, K. Koike, Blocking CXCLs-CXCR2 axis in tumor-stromal interactions contributes to survival in a mouse model of pancreatic ductal adenocarcinoma through reduced cell invasion/migration and a shift of immune-inflammatory microenvironment. *Oncogenesis* **8**, 8 (2019).
16. U. M. Mahajan, E. Langhoff, E. Goni, E. Costello, W. Greenhalf, C. Halloran, S. Ormanns, S. Kruger, S. Boeck, S. Ribback, G. Beyer, F. Dombroswki, F. U. Weiss, J. P. Neoptolemos, J. Werner, J. G. D'Haese, A. Bazhin, J. Peterhansl, S. Pichlmeier, M. W. Buchler, J. Kleeff, P. Ganeh, M. Sendler, D. H. Palmer, T. Kohlmann, R. Rad, I. Regel, M. M. Lerch, J. Mayerle, Immune cell and stromal signature associated with progression-free survival of patients with resected pancreatic ductal adenocarcinoma. *Gastroenterology* **155**, 1625–1639.e2 (2018).
17. S. Boumahdi, F. J. de Sauvage, The great escape: Tumour cell plasticity in resistance to targeted therapy. *Nat. Rev. Drug Discov.* **19**, 39–56 (2020).
18. I. Marigo, S. Zilio, G. Desantis, B. Mlecnik, A. H. R. Agnellini, S. Ugel, M. S. Sasso, J. E. Qualls, F. Kratochvill, P. Zanovello, B. Molon, C. H. Ries, V. Runza, S. Hoves, A. M. Bilocq, G. Bindea, E. M. C. Mazza, S. Bicciato, J. Galon, P. J. Murray, V. Bronte, T cell cancer therapy requires CD40-CD40L activation of tumor necrosis factor and inducible nitric-oxide-synthase-producing dendritic cells. *Cancer Cell* **30**, 377–390 (2016).
19. R. Geiger, J. C. Rieckmann, T. Wolf, C. Basso, Y. Feng, T. Fuhrer, M. Kogadeeva, P. Picotti, F. Meissner, M. Mann, N. Zamboni, F. Sallusto, A. Lanzavecchia, L-Arginine modulates t cell metabolism and enhances survival and anti-tumor activity. *Cell* **167**, 829–842.e13 (2016).
20. R. B. Caldwell, H. A. Toque, S. P. Narayanan, R. W. Caldwell, Arginase: An old enzyme with new tricks. *Trends Pharmacol. Sci.* **36**, 395–405 (2015).
21. Z. F. Kanyo, L. R. Scolnick, D. E. Ash, D. W. Christianson, Structure of a unique binuclear manganese cluster in arginase. *Nature* **383**, 554–557 (1996).
22. M. Pudlo, C. Demougeot, C. Girard-Thernier, Arginase inhibitors: A rational approach over one century. *Med. Res. Rev.* **37**, 475–513 (2017).
23. S. M. Steggerda, M. K. Bennett, J. Chen, E. Emberley, T. Huang, J. R. Janes, W. Li, A. L. MacKinnon, A. Makkouk, G. Marguier, P. J. Murray, S. Neou, A. Pan, F. Parlati, M. L. M. Rodriguez, L. A. Van de Velde, T. Wang, M. Works, J. Zhang, W. Zhang, M. I. Gross, Inhibition of arginase by CB-1158 blocks myeloid cell-mediated immune suppression in the tumor microenvironment. *J. Immunother. Cancer* **5**, 101 (2017).
24. J. Mortier, J. R. C. Prevost, D. Sydow, S. Teuchert, C. Omieczynski, M. Bermudez, R. Frederick, G. Wolber, Arginase structure and inhibition: Catalytic site plasticity reveals new modulation possibilities. *Sci. Rep.* **7**, 13616 (2017).
25. R. Rotondo, G. Barisione, L. Mastracci, F. Grossi, A. M. Orengo, R. Costa, M. Truini, M. Fabbi, S. Ferrini, O. Barbieri, IL-8 induces exocytosis of arginase 1 by neutrophil polymorphonuclears in nonsmall cell lung cancer. *Int. J. Cancer* **125**, 887–893 (2009).
26. S. Rorvig, O. Ostergaard, N. H. Heegaard, N. Borregaard, Proteome profiling of human neutrophil granule subsets, secretory vesicles, and cell membrane: Correlation with transcriptome profiling of neutrophil precursors. *J. Leukoc. Biol.* **94**, 711–721 (2013).
27. R. Rotondo, M. Bertolotto, G. Barisione, S. Astigiano, S. Mandruzzato, L. Ottonello, F. Dallegri, V. Bronte, S. Ferrini, O. Barbieri, Exocytosis of azurophil and arginase 1-containing granules by activated polymorphonuclear neutrophils is required to inhibit T lymphocyte proliferation. *J. Leukoc. Biol.* **89**, 721–727 (2011).
28. G. Sollberger, D. O. Tilley, A. Zychlinsky, Neutrophil extracellular traps: The biology of chromatin externalization. *Dev. Cell* **44**, 542–553 (2018).
29. E. Perez-Figueroa, P. Alvarez-Carrasco, E. Ortega, C. Maldonado-Bernal, Neutrophils: Many ways to die. *Front. Immunol.* **12**, 631821 (2021).
30. H. R. Thiam, S. L. Wong, R. Qiu, M. Kittisopikul, A. Vahabikashi, A. E. Goldman, R. D. Goldman, D. D. Wagner, C. M. Waterman, NETosis proceeds by cytoskeleton and endomembrane disassembly and PAD4-mediated chromatin decondensation and nuclear envelope rupture. *Proc. Natl. Acad. Sci. U.S.A.* **117**, 7326–7337 (2020).
31. X. Zhao, L. Yang, N. Chang, L. Hou, X. Zhou, L. Yang, L. Li, Neutrophils undergo switch of apoptosis to NETosis during murine fatty liver injury via S1P receptor 2 signaling. *Cell Death Dis.* **11**, 379 (2020).
32. J. Cools-Lartigue, J. Spicer, B. McDonald, S. Gowing, S. Chow, B. Giannias, F. Bourdeau, P. Kubes, L. Ferri, Neutrophil extracellular traps sequester circulating tumor cells and promote metastasis. *J. Clin. Invest.* **123**, 3446–3458 (2013).
33. J. Albrengues, M. A. Shields, D. Ng, C. G. Park, A. Ambrico, M. E. Poindexter, P. Upadhyay, D. L. Uyeminami, A. Pommier, V. Kuttner, E. Bruzas, L. Maiorino, C. Bautista, E. M. Carmona, P. A. Gimotty, D. T. Fearon, K. Chang, S. K. Lyons, K. E. Pinkerton, L. C. Trotman, M. S. Goldberg, J. T. Yeh, M. Egeblad, Neutrophil extracellular traps produced during inflammation awaken dormant cancer cells in mice. *Science* **361**, eaao4227 (2018).
34. K. Saegusa, N. Ishimaru, K. Yanagi, R. Arakaki, K. Ogawa, I. Saito, N. Katunuma, Y. Hayashi, Cathepsin S inhibitor prevents autoantigen presentation and autoimmunity. *J. Clin. Invest.* **110**, 361–369 (2002).
35. J. L. Figueiredo, M. Aikawa, C. Zheng, J. Aaron, L. Lax, P. Libby, J. L. de Lima Filho, S. Gruener, J. Fingerle, W. Haap, G. Hartmann, E. Aikawa, Selective cathepsin S inhibition attenuates atherosclerosis in apolipoprotein E-deficient mice with chronic renal disease. *Am. J. Pathol.* **185**, 1156–1166 (2015).
36. E. Jobs, U. Riserus, E. Ingelsson, J. Helmersson, E. Nerpin, M. Jobs, J. Sundstrom, L. Lind, A. Larsson, S. Basu, J. Arnlov, Serum cathepsin S is associated with serum C-reactive protein and interleukin-6 independently of obesity in elderly men. *J. Clin. Endocrinol. Metab.* **95**, 4460–4464 (2010).
37. L. Sevenich, R. L. Bowman, S. D. Mason, D. F. Quail, F. Rapaport, B. T. Elie, E. Brogi, P. K. Brastianos, W. C. Hahn, L. J. Holsinger, J. Massague, C. S. Leslie, J. A. Joyce, Analysis of tumour- and stroma-supplied proteolytic networks reveals a brain-metastasis-promoting role for cathepsin S. *Nat. Cell Biol.* **16**, 876–888 (2014).

38. C. Palermo, J. A. Joyce, Cysteine cathepsin proteases as pharmacological targets in cancer. *Trends Pharmacol. Sci.* **29**, 22–28 (2008).
39. M. M. Mohamed, B. F. Sloane, Multifunctional enzymes in cancer. *Nat. Rev. Cancer* **6**, 764–775 (2006).
40. M. Novinec, R. N. Grass, W. J. Stark, V. Turk, A. Baici, B. Lenarcic, Interaction between human cathepsins K, L, and S and elastins: Mechanism of elastinolysis and inhibition by macromolecular inhibitors. *J. Biol. Chem.* **282**, 7893–7902 (2007).
41. N. Obermajer, Z. Jevnikar, B. Doljak, J. Kos, Role of cysteine cathepsins in matrix degradation and cell signalling. *Connect. Tissue Res.* **49**, 193–196 (2008).
42. V. Gocheva, W. Zeng, D. Ke, D. Klimstra, T. Reinheckel, C. Peters, D. Hanahan, J. A. Joyce, Distinct roles for cysteine cathepsin genes in multistage tumorigenesis. *Genes Dev.* **20**, 543–556 (2006).
43. J. A. Joyce, A. Baruch, K. Chehade, N. Meyer-Morse, E. Giraudo, F. Y. Tsai, D. C. Greenbaum, J. H. Hager, M. Bogyo, D. Hanahan, Cathepsin cysteine proteases are effectors of invasive growth and angiogenesis during multistage tumorigenesis. *Cancer Cell* **5**, 443–453 (2004).
44. K. M. Bell-McGuinn, A. L. Garfall, M. Bogyo, D. Hanahan, J. A. Joyce, Inhibition of cysteine cathepsin protease activity enhances chemotherapy regimens by decreasing tumor growth and invasiveness in a mouse model of multistage cancer. *Cancer Res.* **67**, 7378–7385 (2007).
45. R. E. Burden, J. A. Gormley, T. J. Jaquin, D. M. Small, D. J. Quinn, S. M. Hegarty, C. Ward, B. Walker, J. A. Johnston, S. A. Olwill, C. J. Scott, Antibody-mediated inhibition of cathepsin S blocks colorectal tumor invasion and angiogenesis. *Clin. Cancer Res.* **15**, 6042–6051 (2009).
46. L. Di Costanzo, G. Sabio, A. Mora, P. C. Rodriguez, A. C. Ochoa, F. Centeno, D. W. Christianson, Crystal structure of human arginase I at 1.29-A resolution and exploration of inhibition in the immune response. *Proc. Natl. Acad. Sci. U.S.A.* **102**, 13058–13063 (2005).
47. R. L. Palte, V. Juan, Y. Gomez-Llorente, M. A. Bailly, K. Chakravarthy, X. Chen, D. Cipriano, G. N. Fayad, L. Fayadat-Dilman, S. Gathiaka, H. Greb, B. Hall, M. Handa, M. Hsieh, E. Kofman, H. Lin, J. R. Miller, N. Nguyen, J. O'Neil, H. Shaheen, E. Sterner, C. Strickland, A. Sun, S. Taremi, G. Scapin, Cryo-EM structures of inhibitory antibodies complexed with arginase 1 provide insight into mechanism of action. *Commun. Biol.* **4**, 927 (2021).
48. H. U. Zeilhofer, W. Schorr, Role of interleukin-8 in neutrophil signaling. *Curr. Opin. Hematol.* **7**, 178–182 (2000).
49. K. A. Schalper, M. Carleton, M. Zhou, T. Chen, Y. Feng, S. P. Huang, A. M. Walsh, V. Baxi, D. Pandya, T. Baradet, D. Locke, Q. Wu, T. P. Reilly, P. Phillips, V. Nagineni, N. Gianino, J. Gu, H. Zhao, J. L. Perez-Gracia, M. F. Sanmamed, I. Melero, Elevated serum interleukin-8 is associated with enhanced intratumor neutrophils and reduced clinical benefit of immune-checkpoint inhibitors. *Nat. Med.* **26**, 688–692 (2020).
50. V. Papayannopoulos, Neutrophil extracellular traps in immunity and disease. *Nat. Rev. Immunol.* **18**, 134–147 (2018).
51. A. Teijeira, S. Garasa, M. C. Ochoa, M. Villalba, I. Olivera, A. Cirella, I. Eguren-Santamaria, P. Berraondo, K. A. Schalper, C. E. de Andrea, M. F. Sanmamed, I. Melero, IL8, neutrophils, and NETs in a collusion against cancer immunity and immunotherapy. *Clin. Cancer Res.* **27**, 2383–2393 (2021).
52. C. E. de Andrea, M. C. Ochoa, M. Villalba-Esparza, A. Teijeira, K. A. Schalper, M. Abengozar-Muela, I. Eguren-Santamaria, C. Sainz, S. Sanchez-Gregorio, S. Garasa, M. Ariz, C. Ortiz-de-Solorzano, M. E. Rodriguez-Ruiz, J. L. Perez-Gracia, M. D. Lozano, J. I. Echeveste, M. F. Sanmamed, I. Melero, Heterogenous presence of neutrophil extracellular traps in human solid tumours is partially dependent on IL-8. *J. Pathol.* **255**, 190–201 (2021).
53. M. Munder, H. Schneider, C. Luckner, T. Giese, C. D. Langhans, J. M. Fuentes, P. Kropf, I. Mueller, A. Kolb, M. Modolell, A. D. Ho, Suppression of T-cell functions by human granulocyte arginase. *Blood* **108**, 1627–1634 (2006).
54. F. De Sanctis, R. Trovato, S. Ugel, Anti-telomerase T cells adoptive transfer. *Aging (Albany NY)* **9**, 2239–2240 (2017).
55. S. Sandri, F. De Sanctis, A. Lamolinara, F. Boschi, O. Poffe, R. Trovato, A. Fiore, S. Sartori, A. Sbarbati, A. Bondanza, S. Cesaro, M. Krampera, M. T. Scupoli, M. I. Nishimura, M. Iezzi, S. Sartoris, V. Bronte, S. Ugel, Effective control of acute myeloid leukaemia and acute lymphoblastic leukaemia progression by telomerase specific adoptive T-cell therapy. *Oncotarget* **8**, 86987–87001 (2017).
56. S. Sandri, S. Bobisse, K. Moxley, A. Lamolinara, F. De Sanctis, F. Boschi, A. Sbarbati, G. Fracasso, G. Ferrarini, R. W. Hendriks, C. Cavallini, M. T. Scupoli, S. Sartoris, M. Iezzi, M. I. Nishimura, V. Bronte, S. Ugel, Feasibility of telomerase-specific adoptive T-cell therapy for B-cell chronic lymphocytic leukemia and solid malignancies. *Cancer Res.* **76**, 2540–2551 (2016).
57. D. Bagnara, M. S. Kaufman, C. Calissano, S. Marsilio, P. E. Patten, R. Simone, P. Chum, X. J. Yan, S. L. Allen, J. E. Kolitz, S. Baskar, C. Rader, H. Mellstedt, H. Rabbani, A. Lee, P. K. Gregersen, K. R. Rai, N. Chiorazzi, A novel adoptive transfer model of chronic lymphocytic leukemia suggests a key role for T lymphocytes in the disease. *Blood* **117**, 5463–5472 (2011).
58. N. Glodde, T. Bald, D. van den Boorn-Konijnenberg, K. Nakamura, J. S. O'Donnell, S. Szczepanski, M. Brandes, S. Eickhoff, I. Das, N. Shridhar, D. Hinze, M. Rogava, T. C. van der Sluis, J. J. Ruotsalainen, E. Gaffal, J. Landsberg, K. U. Ludwig, C. Wilhelm, M. Riek-Burchardt, A. J. Muller, C. Gebhardt, R. A. Scolyer, G. V. Long, V. Janzen, M. W. L. Teng, W. Kastenmuller, M. Mazzone, M. J. Smyth, T. Tuting, M. Holzel, Reactive neutrophil responses dependent on the receptor tyrosine kinase c-MET limit cancer immunotherapy. *Immunity* **47**, 789–802.e9 (2017).
59. T. Terashima, D. English, J. C. Hogg, S. F. van Eeden, Release of polymorphonuclear leukocytes from the bone marrow by interleukin-8. *Blood* **92**, 1062–1069 (1998).
60. S. Zacchigna, L. Zentilin, M. Giacca, Adeno-associated virus vectors as therapeutic and investigational tools in the cardiovascular system. *Circ. Res.* **114**, 1827–1846 (2014).
61. P. C. Tumeh, C. L. Harview, J. H. Yearley, I. P. Shintaku, E. J. Taylor, L. Robert, B. Chmielowski, M. Spasic, G. Henry, V. Ciobanu, A. N. West, M. Carmona, C. Kivork, E. Seja, G. Cherry, A. J. Gutierrez, T. R. Grogan, C. Mateus, G. Tomasic, J. A. Glaspy, R. O. Emerson, H. Robins, R. H. Pierce, D. A. Elashoff, C. Robert, A. Ribas, PD-1 blockade induces responses by inhibiting adaptive immune resistance. *Nature* **515**, 568–571 (2014).
62. R. R. Ji, S. D. Chasalow, L. Wang, O. Hamid, H. Schmidt, J. Cogswell, S. Alaparthy, D. Berman, M. Jure-Kunkel, N. O. Siemers, J. R. Jackson, V. Shahabi, An immune-active tumor microenvironment favors clinical response to ipilimumab. *Cancer Immunol. Immunother.* **61**, 1019–1031 (2012).
63. N. Jacquelot, M. P. Roberti, D. P. Enot, S. Rusakiewicz, N. Ternes, S. Jegou, D. M. Woods, A. L. Sodre, M. Hansen, Y. Meirow, M. Sade-Feldman, A. Burra, S. S. Kwek, C. Flament, M. Messaoudene, C. P. M. Duong, L. Chen, B. S. Kwon, A. C. Anderson, V. K. Kuchroo, B. Weide, F. Aubin, C. Borg, S. Dalle, O. Beatrix, M. Ayyoub, B. Balme, G. Tomasic, A. M. Di Giacomo, M. Maio, D. Schadendorf, I. Melero, B. Dreno, A. Khammari, R. Dummer, M. Levesque, Y. Koguchi, L. Fong, M. Lotem, M. Baniyash, H. Schmidt, I. M. Svane, G. Kroemer, A. Marabelle, S. Michiels, A. Cavalcanti, M. J. Smyth, J. S. Weber, A. M. Eggermont, L. Zitvogel, Predictors of responses to immune checkpoint blockade in advanced melanoma. *Nat. Commun.* **8**, 592 (2017).
64. C. H. Chang, J. Qiu, D. O'Sullivan, M. D. Buck, T. Noguchi, J. D. Curtis, Q. Chen, M. Gindin, M. M. Gubin, G. J. van der Windt, E. Tonc, R. D. Schreiber, E. J. Pearce, E. L. Pearce, Metabolic competition in the tumor microenvironment is a driver of cancer progression. *Cell* **162**, 1229–1241 (2015).
65. A.-A. M. Líndez, I. Dunand-Sauthier, M. Conti, F. Gobet, N. Núñez, J. T. Hannich, H. Riezman, R. Geiger, A. Piersigilli, K. Hahn, S. Lemeille, B. Becher, T. De Smedt, S. Hugues, W. Reith, Mitochondrial arginase-2 is a cellautonomous regulator of $CD8^+$ T cell function and antitumor efficacy. *JCI Insight* **4**, e132975 (2019).
66. P. J. Murray, Amino acid auxotrophy as a system of immunological control nodes. *Nat. Immunol.* **17**, 132–139 (2016).
67. J. Oberlies, C. Watzl, T. Giese, C. Luckner, P. Kropf, I. Muller, A. D. Ho, M. Munder, Regulation of NK cell function by human granulocyte arginase. *J. Immunol.* **182**, 5259–5267 (2009).
68. P. Lacy, The role of Rho GTPases and SNAREs in mediator release from granulocytes. *Pharmacol. Ther.* **107**, 358–376 (2005).
69. L. Yang, Q. Liu, X. Zhang, X. Liu, B. Zhou, J. Chen, D. Huang, J. Li, H. Li, F. Chen, J. Liu, Y. Xing, X. Chen, S. Su, E. Song, DNA of neutrophil extracellular traps promotes cancer metastasis via CCDC25. *Nature* **583**, 133–138 (2020).
70. R. E. Burden, J. A. Gormley, D. Kuehn, C. Ward, H. F. Kwok, M. Gazdoiu, A. McClurg, T. J. Jaquin, J. A. Johnston, C. J. Scott, S. A. Olwill, Inhibition of cathepsin S by Fsn0503 enhances the efficacy of chemotherapy in colorectal carcinomas. *Biochimie* **94**, 487–493 (2012).
71. W. N. Liu, S. Y. Fong, W. W. S. Tan, S. Y. Tan, M. Liu, J. Y. Cheng, S. Lim, L. Suteja, E. K. Huang, J. K. Y. Chan, N. G. Iyer, J. P. S. Yeong, D. W. Lim, Q. Chen, Establishment and characterization of humanized mouse NPC-PDX model for testing immunotherapy. *Cancer* **12**, 1025 (2020).
72. F. P. Veras, M. C. Pontelli, C. M. Silva, J. E. Toller-Kawahisa, M. de Lima, D. C. Nascimento, A. H. Schneider, D. Caetite, L. A. Tavares, I. M. Paiva, R. Rosales, D. Colon, R. Martins, I. A. Castro, G. M. Almeida, M. I. F. Lopes, M. N. Benatti, L. P. Bonjorno, M. C. Giannini, R. Luppino-Assad, S. L. Almeida, F. Vilar, R. Santana, V. R. Bollela, M. Auxiliadora-Martins, M. Borges, C. H. Miranda, A. Pazin-Filho, L. L. P. da Silva, L. D. Cunha, D. S. Zamboni, F. Dal-Pizzol, L. O. Leiria, L. Siyuan, S. Batah, A. Fabro, T. Mauad, M. Dolhnikoff, A. Duarte-Neto, P. Saldiva, T. M. Cunha, J. C. Alves-Filho, E. Arruda, P. Louzada-Junior, R. D. Oliveira, F. Q. Cunha, SARS-CoV-2-triggered neutrophil extracellular traps mediate COVID-19 pathology. *J. Exp. Med.* **217**, e20201129 (2020).

Acknowledgments: We thank the patients who contributed to the study and research nurses for collecting patients' samples. We thank F. Pesavento and O. Poffe, Department of Medicine, Immunology Section, University of Verona and N. Sperandio, G. Bonizzato, and S. Grimaldi, ARC-Net Centre for Applied Research on Cancer, University of Verona, for technical work on patients' tumor tissue; G. Zulianello, General and Pancreatic Surgery, Pancreas Institute, University of Verona, for assistance with patients. We acknowledge the contribution of "Centro Piattaforme Tecnologiche" of the University of Verona, particularly the imaging, MS, spectroscopy,

diffractometry, and molecular interaction platforms. **Funding:** The research reported in this publication was supported in part by the Cancer Research Institute, Clinic and Laboratory Integration Program, CLIP 2017 to V.B.; the Italian Association for Cancer Research (AIRC) (23788 and 12182) to V.B.; Cariverona Foundation (Project Call, 2017) to V.B.; Euronanomed III (Joint Translational Call 2017, Project Resolve) to V.B.; PRIN program of Italian Ministry of Education, University and Research (MIUR, CUP: B38D19000260006) to V.B.; and Ricerca Finalizzata 2019, Ministry of Health, project code RF-2019-12369251, to V.B. and S.M. **Author contributions:** S.C. planned the experiments; performed the flow cytometric, biochemical analysis, and animal studies; analyzed the data; and wrote the manuscript. R.M.B. performed purification of human cells, imaging, and biochemical analysis. G.F. performed biochemical experiments. A.A. performed the flow cytometric analysis. M.F. performed biochemical experiments. R.T., F.D.S., and S.U. analyzed animal experiments. J.C. supplied recombinant proteins. M.G. supplied AAV9. R.L. supplied patients' tumor tissue. A.S. supplied patients' tumor tissue. B.R. supplied patients' tumor tissue. S.P. supplied patients' blood. R.S. supplied patients' blood. G.L. supplied patients' blood. C.B. supplied patients' blood. S.M. supplied Abs. S.F. supervised some biochemical experiments. V.B. conceptualized and wrote the manuscript. The initial draft was written by S.C. and V.B. S.C., R.M.B., and V.B participated in reviewing and editing of the manuscript. **Competing interests:** V.B. was a past consultant for IO Biotech ApS, Codiak BioSciences Inc., and ELPIS Biopharmaceuticals. S.U. received a research grant from IO Biotech ApS. The authors declare that they have no other competing interests. **Data and materials availability:** All data associated with this study are present in the paper or the Supplementary Materials. Requests for hARG1 mAb should be directed to V.B. and S.M. and will be made available after completion of a material transfer agreement.

Submitted 11 May 2022
Resubmitted 14 September 2022
Accepted 22 February 2023
Published 15 March 2023
10.1126/scitranslmed.abq6221

Science Translational Medicine

Neutralization of NET-associated human ARG1 enhances cancer immunotherapy

Stefania Can, Roza Maria Barouni, Marina Fabbi, John Cuozzo, Giulio Fracasso, Annalisa Adamo, Stefano Ugel, Rosalinda Trovato, Francesco De Sanctis, Mauro Giacca, Rita Lawlor, Aldo Scarpa, Borislav Rusev, Gabriella Lionetto, Salvatore Paiella, Roberto Salvia, Claudio Bassi, Susanna Mandruzzato, Silvano Ferrini, and Vincenzo Bronte

Sci. Transl. Med., **15** (687), eabq6221.
DOI: 10.1126/scitranslmed.abq6221

Science Translational Medicine (ISSN) is published by the American Association for the Advancement of Science. 1200 New York Avenue NW, Washington, DC 20005. The title *Science Translational Medicine* is a registered trademark of AAAS.